STUDY OF IMAGE QUALITY IMPROVEMENT TECHNIQUES

A THESIS

SUBMITTED TO THE DELHI TECHNOLOGICAL UNIVERSITY

FOR THE AWARD OF THE DEGREE OF

DOCTOR OF PHILOSOPHY

IN

Electronics and Communication Engineering

SUBMITTED BY

KULDEEP SINGH

DEPARTMENT OF ELECTRONICS & COMMUNICATION ENGINEERING

DELHI TECHNOLOGICAL UNIVERSITY

DELHI- 110042 (INDIA)

DECEMBER 2015

DELHI TECHNOLOGICAL UNIVERSITY

CERTIFICATE

This is to certify that the thesis entitled **"STUDY OF IMAGE QUALITY IMPROVEMENT TECHNIQUES"** being submitted by Kuldeep Singh (Reg. No.: 2K11/PhD/E&C/04) for the award of degree of Doctor of Philosophy to the Delhi Technological University is based on the original research work carried out by him. He has worked under my supervision and has fulfilled the requirements which to my knowledge have reached the requisite standard for the submission of this thesis. It is further certified that the work embodied in this thesis has neither partially nor fully submitted to any other university or institution for the award of any degree or diploma.

Prof. Rajiv Kapoor
(Supervisor)
Professor, Deptt. of Electronics & Comm. Engg.
Delhi Technological University

ACKNOWLEDGEMENT

As the curtains draw on my journey as a PhD student, and I look forward to embarking on my career, I have many people to thank. Foremost of them is my supervisor, Prof. Rajiv Kapoor, without whom this thesis would not have been possible. His substantial and thorough approach, together with his genuine interest in the research subject, turned my research work into a great experience. Our interactions have helped transform me into the researcher that I am today.

I would like to thank Mr. Gurjit S. Walia and Mr. Dinesh Kr. Viswakarma for their kind help and wisdom. With great pleasure I express my heartfelt gratitude for their advice, fruitful discussions, numerous suggestions, constructive criticism, and constant support throughout the period of my research. Throughout my PhD research journey under graduate students of DTU had shown tremendous research interest. I would always admire their enthusiasm. I would also thank my colleagues Mr. Sanjay Motia and Mr. Sandeep Kumar for their support in reviewing my research papers and providing me their valuable comments which enriched my research.

Above all, my heartfelt thanks go to my parents, my son (Kushagra) and my wife (Komal). I know I wouldn't finish the PhD without their non-stopping love, encouragement and support. I admire my wife’s sincere efforts in providing support at various stages.

Finally, I thank to all those who helped and supported me. Thank you so much!

ABSTRACT

Image quality improvement has always been a topic of interest for the researchers. The ultimate objective of image quality improvement in a broad sense is to improve a degraded image that can express all the information of the scene. The need for the image quality improvement is necessitated because of the limited hardware capabilities of image capturing devices, the uneven lighting conditions, and noisy environment. In this scenario, post-processing is needed to improve the quality of the acquired image. This thesis explores new algorithms for image quality improvement.

This thesis addresses several open questions: a) How do the repetitive geometric structures such as ridges and valleys in fingerprints can be exploited for better sparse representation of fingerprint images? b) How can denoising and superresolution algorithms be incorporated in traditional enhancement methods to help in reliable and accurate fingerprint matching? c) How can histogram equalization be effective in contrast enhancement of low exposure images?

In an attempt to answer these questions, this thesis explores three aspects of image quality improvement i.e. denoising, super-resolution and contrast enhancement. Being motivated from recent advancements in sparse coding based image processing applications, a novel ridge orientation based clustered sparse dictionary is proposed for exploiting self-similarity in fingerprint images which often contains many repetitive geometric structures such as ridges and valleys. Instead of having a single dictionary, the proposed dictionary-learning method clusters the training patches into smooth, non-

dominant orientation and dominant orientation groups. The use of sub-dictionaries based on dominant orientation best describes the underlying image data. This also improves the effectiveness of sparse modeling of information in a fingerprint image in the form of local ridge patterns and thus further improves denoising and super-resolution performance. Two novel fingerprint image denoising and super-resolution algorithms based on ridge orientation based clustered sparse dictionary are proposed.

The fingerprint denoising approach undergoes three steps i.e. Ridge orientation based patch clustering, Sub-dictionary learning and sparse coefficient calculation. While reconstructing the denoised image in the final step, the minimum residual error criterion is used for choosing sub-dictionary that best suits for a particular patch.

The fingerprint super-resolution algorithm involves learning of coupled sub-dictionaries each for low and high-resolution training patch groups that are clustered based on dominant orientation. In the final step of superresolution, the iterative back projection is applied to eliminate the discrepancy in the estimate due to noise or inaccuracy in the sparse representation.

To evaluate the performance of proposed fingerprint denoising and super-resolution methods, a validation methodology consisting of three experiments i.e. comparison based on image quality measures, visual quality, and fingerprint matching is devised. The performance comparison results show that the proposed methods achieve better results in comparison with other methods and will help in improving the performance of fingerprint-identification systems.

This research also addresses the problem of low exposure imaging through contrast enhancement using histogram equalization. A novel Exposure based Sub-Image Histogram Equalization (ESIHE) method for contrast enhancement is proposed which partitions the image into sub-images i.e. under-exposed and over-exposed. The individual histograms of sub-images are equalized independently. The two recursive variants of ESIHE are also proposed that proves to be very effective for improvement in the quality of images acquired in low light conditions such as underwater sequences or night vision. The first method is Recursive Exposure based sub-image histogram equalization (R-ESIHE) that recursively performs ESIHE method till the exposure residue among successive iteration is less than a predefined threshold. The second method is named as Recursively separated Exposure based sub-image histogram equalization (RS-ESIHE) that partitions the image histogram recursively. Each sub-histogram is further partitioned based on their respective exposure thresholds, and finally all the sub-histograms are equalized individually. The experimental results show that the proposed methods efficiently handled the low exposure image enhancement problem that was not addressed by earlier HE based methods.

Another variant of histogram equalization i.e. Median-Mean based sub-image clipped histogram equalization (MMSICHE) method is developed to addresses the problem of preservation of mean brightness, entropy and control on the enhancement rate simultaneously. The algorithm consists of three steps, namely median and mean calculation, Histogram Clipping and Histogram Subdivision & Equalization. The important factors for accomplishing the objective by MMSICHE method can be summarized as (i) Bisecting the image based on the median value plays the role in

maximizing entropy and natural enhancement. (ii) Sub-dividing the image into four sub-images based on mean intensity plays the role for brightness preservation. (iii) Histogram clipping approach provides the feature of control on over enhancement. The simulation results show that MMSICHE method avoids excessive enhancement and produces images with a natural appearance.

LIST OF PUBLICATIONS

1. **Kuldeep Singh**, Rajiv Kapoor, Raunaq Nayar, "Fingerprint denoising using ridge orientation based clustered dictionaries", **Neurocomputing** (**Elsevier**) 167(2015)418-423 (DOI:10.1016/j.neucom.2015.04.053)
2. **Kuldeep Singh**, Rajiv Kapoor, "Image enhancement using Exposure based Sub-image Histogram Equalization", **Pattern Recognition Letters** (**Elsevier**) 36 (2014) 10 – 14 (DOI:10.1016/j.patrec.2013.08.024)
3. **Kuldeep Singh**, Anubhav Gupta, Rajiv Kapoor, "Fingerprint image super-resolution via ridge orientation based clustered coupled sparse dictionaries", **Journal of Electronic Imaging** (**SPIE**) 20(4) (2015) (DOI:10.1117/1.JEI.24.4.043015)
4. **Kuldeep Singh**, Rajiv Kapoor, "Image enhancement via Median-Mean Based Sub-Image-Clipped Histogram Equalization", **Optik- Int. J. Light Electron Opt**., (**Elsevier**) 125 (2014) 4646-4651 (DOI:10.1016/j.ijleo. 2014.04.093)
5. **Kuldeep Singh**, Rajiv Kapoor, Sanjeev Kr. Sinha, "Enhancement of low Exposure Images via Recursive Histogram Equalization Algorithms", **Optik- Int. J. Light Electron Opt.,** (**Elsevier**) 126 (2015) 2619–2625 (DOI:10.1016/j.ijleo.2015.06.060)

TABLE OF CONTENT

LIST OF TABLES

LIST OF FIGURES

LIST OF ABBREVIATIONS

AMBE	Absolute Mean Brightness Error
BGL	Background Gray Level
CDF	Cumulative Distribution Function
DET	Detection Error Tradeoff
EER	Equal Error Rate
ESIHE	Exposure Based Sub-Image Histogram Equalization
FAR	False Acceptance Ratio
FRR	False Rejection Ratio
HE	Histogram Equalization
IQM	Image Quality Measure
NLM	Non-Local Means
PDF	Probability Density Function
PSNR	Peak Signal to Noise Ratio
SSIM	Structural Similarity
SVD	Singular Value Decomposition

CHAPTER 1

INTRODUCTION

The need for the image quality improvement is necessitated because of the limited hardware capabilities of image capturing devices, the uneven lighting conditions, and noisy environment. Captured images are often not of desired quality and post-processing is needed to improve the quality of the acquired image. Software-based improvement tools are more popular as they are usually hardware independent and widely applicable. These tools improve the visual appearance of the image for better interpretation to assist in computer vision tasks i.e. analysis, segmentation, object detection, tracking, pattern recognition, biometric recognition etc. This chapter discusses different aspects of image quality improvement techniques. A brief introduction on sparse representation based denoising and superresolution is also presented. In the final section, the main contribution and organization of thesis is elaborated.

1.1 Background

Practically there are two main aspects of designing an image quality improvement algorithm. The first one is the objective aspect where the missing ingredients of an image are estimated, and the degraded image is restored close to the original scene. The second is the subjective aspect where the degraded image is enhanced, and aesthetics are improved to please the human visual system. A better quality image is perceived to have

higher contrast, better resolution, lesser noise, no blurring, less visual artifacts, and contains contextually meaningful information so that it can be better used for analysis.

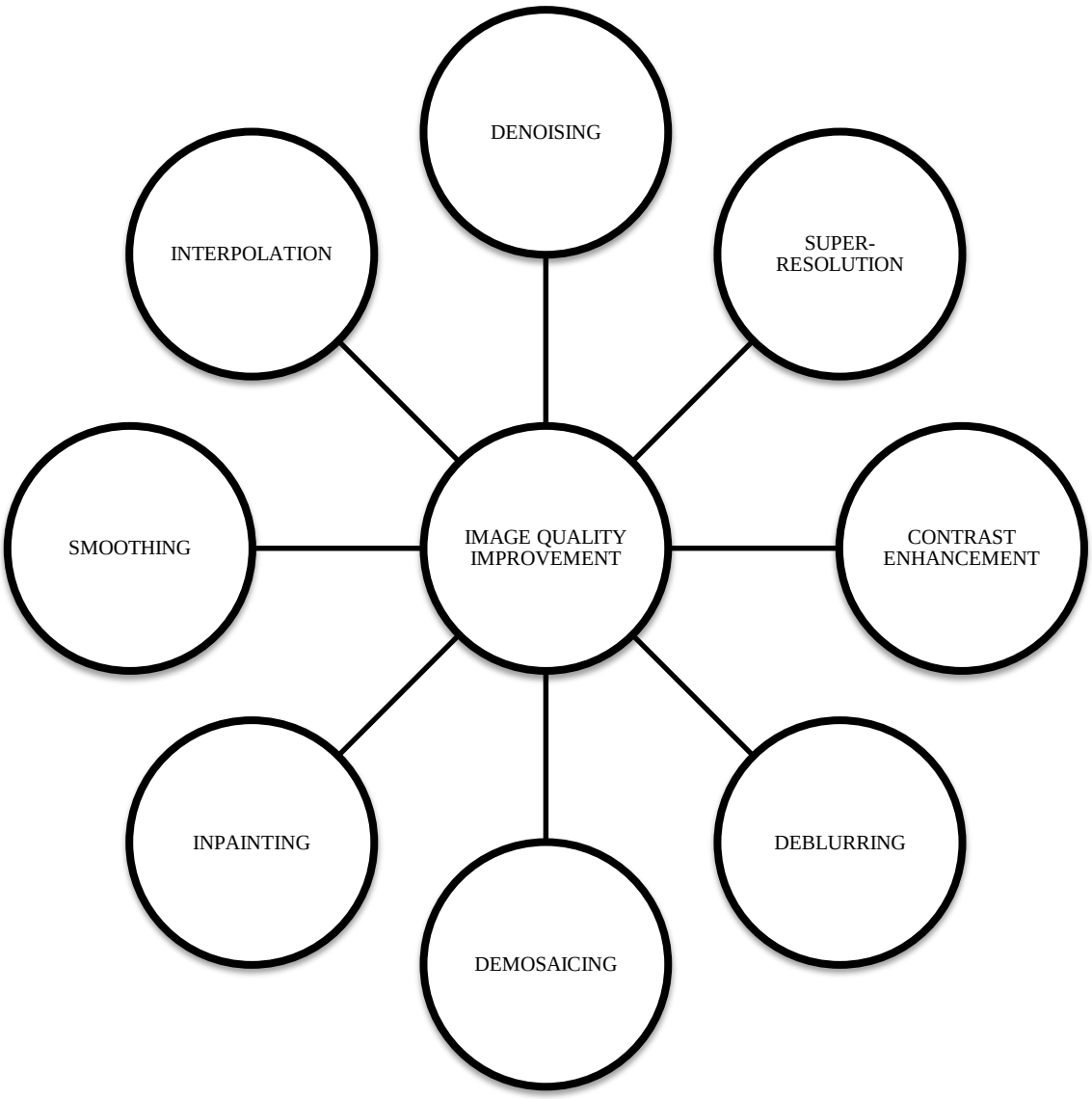

Figure 1.1 Image quality improvement techniques

Software-based image quality improvement techniques are more popular as they are usually hardware independent and widely applicable. The key techniques for quality improvement of an image include denoising, contrast enhancement, super-resolution, deblurring, demosaicing, inpainting, smoothing, interpolation, and so forth. Figure 1.1 depicts various algorithms that contribute in image quality improvement. These tools improve the visual appearance of the image for better visual interpretation to assist in subsequent image processing tasks (analysis, detection, segmentation, and recognition).

Image quality improvement aims to reproduce a high-quality image from its degraded measurement. Reconstructing a high-quality image from observed degraded version is an ill-posed inverse problem. This inverse problem can modeled as

$$Y = \Psi\psi X + V \tag{1.1}$$

where X is the original high-quality image, and Ψ are ψ quality degradation operators, and V is Gaussian noise. This inverse problem in Equation 1.1 becomes

- Denoising problem when Ψ and ψ are identities;
- Deblurring problem when ψ is a blurring operator and Ψ is identity and
- Super-resolution (single-image) when Ψ and ψ are down-sampling and blurring operator respectively.

For solving the ill-posed linear inverse problem in Equation 1.1, image prior knowledge is usually utilized for regularizing the solution to the following minimization problem

$$\underset{X}{\operatorname{argmin}} \ \|\Psi\psi X - Y\|_2^2 + \ \lambda P_r(X) \tag{1.2}$$

The first term is l_2 data fidelity term and second term $P_r(X)$ is called the regularization term denoting image prior and λ is the regularization parameter. Many regularization terms [**1**] [**2**] [**3**] has been purposed in past. Although these regularization terms are highly effective in preserving edges, however, they usually smear out image details and cannot deal well with fine structures [**4**].

In recent years, sparsity-based regularization has emerged as effective prior and has achieved excellent results in various image processing applications, such as denoising [**5**], deblurring [**6**], and super-resolution [**7**]. The sparse model is motivated from the idea that an image can be approximately coded as a linear combination of few columns (atoms) of an over-complete dictionary learned from natural images. The traditional dictionaries i.e. contourlet [**8**], curvelets [**9**], wedgelet [**10**], bandlets [**11**], etc. are based are not adaptive to the images, however; the learned dictionary being better adapted to the images enhances the sparsity and show impressive performance improvement. The matching pursuit [**12**] and the basis pursuit [**13**] class of sparse coding algorithm gave rise to the ability to address the image quality improvement problem as a direct sparse decomposition technique over redundant dictionaries.

In this research three aspects of image quality improvement i.e. sparse representation based super-resolution, sparse representation based denoising and contrast enhancement are mainly explored. The application of super-resolution and denoising in the field of fingerprint quality improvement is extensively studied in this research.

1.2 Sparse Representation based Image Denoising

The goal of quality improvement through image denoising algorithm is to suppress noise while producing sharp images without loss of finer details. The classic image denoising problem is modeled by assuming an ideal image being captured in the presence of an additive zero-mean white and homogeneous Gaussian noise with standard deviation. These days, images captured by imaging devices are invariably corrupted by noise. With the advent of high-resolution modern cameras, signal sensors are becoming increasingly dense hence with same aperture size, noise suppression has become more relevant [**14**].

The concept of sparse based image denoising is motivated from the idea that a high-quality image X can be approximately coded as a linear combination of few columns (atoms) of an over-complete dictionary. Overcomplete dictionaries contain more atoms than the dimension of the signal. A signal $X = \{x_1, x_2 \ldots\ldots, x_n\}$ is said to be sparse when very few of entries x_i possess non-zero values. Sparse representation computes the summation of the constituent atoms weighted with their sparse coefficients vector. However, computing such sparse codes within overcomplete dictionaries is non-trivial, in particular because the decomposition of an image in terms of atoms of an overcomplete dictionary is not unique. Processing the whole image as a large vector is numerically cumbersome, Elad & Aharon [**5**], proposed breaking down the image into smaller patches and learning a dictionary of patch-sized atoms. Handling high dimensionality of data in image denoising is a major challenge, the patch-based method models the patches with relatively lower dimension, seems the effective solution to tackle this problem.

1.2.1 Sparse Reconstruction Model for Image Denoising

Given an image observation patch of size $\sqrt{p} \times \sqrt{p}$ ordered lexicographically as column vector $x \in R^p$ and a sparsifying dictionary $\varphi = \{\varphi_1, \varphi_2 \ldots\ldots, \varphi_c\} \in R^{n \times M}$ (the

columns $\varphi_i \in R^M$ represent the atoms), sparse representation refer to finding a coefficient vector $\alpha \in R^p$ in the domain spanned by the dictionary φ while synthesizing following equation

$$\hat{\alpha} \in \underset{\alpha}{\operatorname{argmin}} \|\alpha\|_0 \; subject\ to\ x = \varphi\alpha \tag{1.3}$$

The solution is indeed very sparse where $\|\hat{\alpha}\|_0 \ll n$. While synthesizing approximately, the equality constraint in Equation (1.3) can be replaced by a l_2 norm inequality constraint.

$$\hat{\alpha} \in \underset{\alpha}{\operatorname{argmin}} \|\alpha\|_0 \; subject\ to\ \|x - \varphi\alpha\|_2 \leq \varepsilon_1 \tag{1.4}$$

where ε controls the misfitting between observed and recovered signal $\hat{x} = \varphi\hat{\alpha}$. Now considering a patch y, noisy version of x, contaminated with additive white Gaussian noise. The denoising of noisy patch y can be formulated as following optimization problem.

$$\hat{\alpha} \in \underset{\alpha}{\operatorname{argmin}} \|\alpha\|_0 \; subject\ to\ \|y - \varphi\alpha\|_2^2 \leq \varepsilon_2 \tag{1.5}$$

The denoised patch can be recovered as $\hat{x} = \varphi\hat{\alpha}$. The optimization problem in Equation (1.5) can also be reformulated in its unconstrained penalized form.

$$\hat{\alpha} = \underset{\alpha}{\operatorname{argmin}} \|y - \varphi\alpha\|_2^2 + \beta\|\alpha\|_0 \tag{1.6}$$

The solution of Equation 1.5 is NP-hard problem; however, l_1-norm can be used to make it computationally tractable (convex) as an alternate to l_0-norm (non-convex). Matching pursuit [**12**] class of algorithms that include orthogonal matching pursuit (OMP) [**15**],

basis pursuit (BP) [**13**] and gradient pursuit (GP) provide efficient and computationally tractable solutions to the optimization problem.

1.3 Sparse Representation based Image Superresolution

Resolution enhancement algorithms are essential constituents in the field of medical imaging, satellite imaging and where diagnosis or analysis from low-quality images can be extremely difficult [**7**]**.** Quality improvement through image super-resolution (SR) offers the promise of overcoming some of the inherent resolution limitations of low-cost imaging sensors (e.g. cell phone or surveillance cameras).

Classical SR methods attempted to restore a high-resolution (HR) image by combining multiple low-resolution (LR) observations. Due to difficulty in obtaining image sequences for same LR image, new age methods use information from the single LR observation to reconstruct HR image based on training sets. Due to this reason, training set based single-image super-resolution (SISR) methods have attracted more attention in recent years Superresolution of biometric images may also prove effective in improving the performance of identity recognition process. Specifically in crime investigation [**16**] scenarios, superresolution of fingerprints can be very effective where acquired images are of very low resolution.

Recently, super-resolution methods based on learning techniques are a rapidly evolving field. This attention is based on the assumption that an image can be restored as a linear combination of atoms from an overcomplete dictionary.

1.3.1 Coupled Dictionary based Single Image Superresolution

Instead of working on single dictionary here coupled dictionaries, D_h for high-resolution patches, and D_l for low-resolution ones is learned [**7**]. The sparse coding of a low-resolution patch in terms of D_l can be directly applied to recover the corresponding high-resolution patch using D_h.

Using an overcomplete low resolution dictionary $D_l \in R^{n \times N}$ of N atoms, the observed low resolution image patches of size $\sqrt{n} \times \sqrt{n}$ can be represented as a sparse linear combination of atoms as below:

$$y_i = D_l.\alpha \; ; \; \|\alpha\|_0 < \varepsilon \tag{1.7}$$

where y_i is the linear vector of LR image is patch and $\alpha \in R^N$ is a coefficient vector. By training a set of HR and LR coupled dictionaries $\{D_h, D_l\}$, it can be assumed that the sparse representation of a low-resolution patch in terms of D_l can be directly used to recover the corresponding high-resolution patch x_i from D_h i.e.

$$x_i = D_h.\alpha \tag{1.8}$$

where coupled dictionary means that each atom in D_h has its corresponding low-resolution version in D_l and vice versa [**17**].

The above problem can be modeled as the following optimization function [**7**]

$$min\|\alpha\|_0 \; s.t. \|GD_l\alpha - Gy_i\|_2^2 \leq \epsilon \tag{1.9}$$

where G is a gradient feature extraction operator i.e.

$$G = \left\{\frac{\partial I(u,v)}{\partial u}, \frac{\partial I(u,v)}{\partial v}, \frac{\partial^2 I(u,v)}{\partial u^2}, \frac{\partial^2 I(u,v)}{\partial v^2}\right\}^T \tag{1.10}$$

According to results in [**18**], the l_0-norm of above optimization problem can be relaxed as the l_1-norm, and the optimization function can be reformulated as:

$$min_\alpha \|GD_l\alpha - Gy_i\|_2^2 + \mu\|\alpha\|_1 \tag{1.11}$$

Where μ is fidelity factor, which regularizes the sparsity. The above optimization problem can be solved using LARS [**19**] algorithm with LASSO [**20**] modification.

1.4 Contrast Enhancement

Contrast enhancement techniques are widely used for improving the visual quality of low contrast images. Contrast enhancement improves the visual quality of an image as well as the specific image features for further processing and analysis by a computer vision system. There are several reasons behind poor contrast of an image [**21**].

- Poor quality of the used imaging device,
- Lack of expertise of the operator, and
- Low-light environment (e.g., in a dark room or during night time), at the time of acquisition

Due to above mentioned factors, the complete dynamic range remains under-utilized. As a result, such images possess poor contrast and may not reveal all the details in the captured scene, and may have an unnatural look. Contrast enhancement techniques find application in areas ranging from consumer electronics, medical image processing to radar and sonar image processing.

1.5 Fingerprint Quality Improvement

This research has also addressed the problem of quality improvement of fingerprint images. Automatic fingerprint identification systems (AFIS) are an integral part of man-machine interface systems for verification of individual's identity. Fingerprints have proved to be an effective biometric identifier and are extensively employed in forensic science [**16**] in criminal investigations, and in biometric systems such as civilian as well

as commercial identification devices [**22**]. The efficiency of fingerprint recognition systems is largely dependent on the quality of input fingerprint image [**23**]. There could be various factors behind the substandard quality of fingerprint images, such as efficiency of the image acquisition sensor, corrupted with noise due to variation in skin and impression condition and so on. Image quality improvement process helps in reducing the probability of error in the recognition process. Due to these reasons, quality improvement of fingerprint image has always been an active research area to support AFIS.

1.6 Thesis Organization and Contributions

In this thesis, various novel image quality improvement algorithms are developed. The thesis work is divided into different chapters. Chapter wise contribution of the thesis is as follows:

Chapter 2: Literature Review

- A detailed and exhaustive literature survey is presented for various image quality improvement techniques using denoising, superresolution, and contrast enhancement.
- Based on the literature survey research gaps are identified, and research objective of the thesis are formulated.

Chapter 3: Sparse Representation based Fingerprint Denoising

- A novel algorithm is proposed for constructing ridge orientation based sparse sub-dictionary that exploits the self-similarity among fingerprint patches.

- Fingerprint denoising algorithm is proposed using ridge orientation based sub-dictionaries and performance of proposed method is compared with other state of the art denoising methods on public fingerprint databases.

Chapter 4: Sparse Representation based Fingerprint Superresolution

- A novel method is described for fingerprint superresolution. This method utilizes the concept of ridge orientation based clustered coupled dictionary to enhance the superresolution performance.
- Exhaustive performance comparison of proposed superresolution algorithm is presented not only in terms of image quality measures (PSNR and SSIM) but also in terms of fingerprint recognition accuracy.

Chapter 5: Contrast Enhancement using Histogram Equalization

- A new algorithm named as MMSICHE is presented for achieving the multi-objective of preservation of mean brightness, entropy, and control on the enhancement rate simultaneously.
- Novel exposure based sub-image histogram equalization (ESIHE) algorithm is proposed to address the problem of low-exposure imaging under low light or underwater conditions.
- Two recursive variants of ESIHE algorithm are also developed to increase the robustness of ESIHE method for low-exposure images.
- Detailed performance evaluation is performed for proposed methods in terms of image quality measures as well as visual quality inspection.

Chapter 6: Conclusion and Future Scope of Work

- Conclusions of proposed image quality methods are drawn in this chapter.
- A detailed discussion on possible avenues of future scope work is presented.

CHAPTER 2

LITERATURE REVIEW

This chapter presents the summary of relevant image quality improvement methods present in the literature. The review is focused on sparse representation based denoising and superresolution with application to fingerprint images. A detailed literature review of histogram equalization based contrast enhancement methods is also presented.

2.1 Image Denoising

Due to the increase of image sensors per unit area, imaging devices can be interrupted by noise. Therefore, denoising technique is an important step for improving the visual quality of images. The image denoising algorithms can be roughly classified into two categories i.e. spatial filtering methods and transform domain filtering methods [**24**].

Spatial filtering methods attempt to exploit the similarities between either pixels or patches by utilizing the spatial correlations. A wide variety of noise reducing spatial filters has been proposed in the past i.e. Wiener filter [**25**], Gabor filter [**26**], Anisotropic filtering [**27**], Total variation minimization [**1**] [**28**] etc. These filters are local in the sense that the filter coefficients are restricted by spatial distance. On the contrary to local filters, Nonlocal Means (NLM) [**29**] algorithm make use of the self-similarity of natural images in a global manner and obtains a denoised patch by weighted averaging all other similar patches in the same image. Considering the effectiveness of NLM method various

improvement of NLM were proposed [**30**] [**31**] [**32**] [**33**]. Although nonlocal spatial methods deal high noise efficiently but the major drawback of NLM is that it introduce artifacts such as over-smoothing.

Transform domain methods transform the image into other domains, in which similarities of transformed coefficients are employed. The main motivation of denoising in the transform domain is that coefficients representing noise can be easily separated out from the image using shrinkage or thresholding methods. In the image denoising literature, a variety of transform domains has been proposed to suppress noise from an image. Among the many transform domain approaches present in literature, the space-frequency localization property of the wavelet domain makes it the most popular choice. There are numerous wavelet based denoising algorithms [**34**] [**35**] [**36**] [**37**] [**38**] present in literature to estimate image from its degraded version. Other popular transform domain filters are curvelets [**39**], contourlets [**40**], and bandelets [**41**]. Recently the third category of image denoising has evolved i.e. dictionary based denoising. The key difference with transform domain is that instead of representing images with fixed basis functions dictionary based methods adapts from the training images [**5**].

In this thesis, a specific approach i.e. sparsity-based image denoising is being focused. Elad & Aharon [**5**] addressed image denoising problem using K-SVD algorithm [**42**] of optimal overcomplete dictionary construction. In this method, each patch is denoised by representing a patch as a linear combination of only a few atoms in the dictionary. Mairal *et al.* [**43**] proposed multi-scale global dictionaries for performance improvement of dictionary learning. Chatterjee and Milanfar [**14**] proposed locally learned dictionaries (K-LLD) for image denoising, which performs clustering based on

similar geometric structures and employs local weight functions as features. Xiaoqiang *et al.* [**44**] proposed a Bayesian-based sparse coding algorithm, which employs spike and slab prior providing accurate prediction and effective sparse representation. Zhang *et al.* [**45**] introduced a new approach of image denoising, which creates 2D dictionary based on the self-similarity inherent in the images. This method relies on the idea that if a group of similar patches are assembled in matrix form, then there exist linear correlations among both columns and rows. Yang *et al.* [**46**] proposed new dictionary learning approach for image noise reduction, which exploits structural similarities of the image. The Wiener filter forms the basis of another celebrated denoising method i.e. BM3D [**47**] proposed by Dabov *et al*. BM3D algorithm is a unified framework of dictionary learning and structural clustering, which yields excellent PSNR performance. Considering the promising results of sparse representation based image denoising algorithms, addressing the fingerprint denoising with these algorithms will be an interesting research area.

2.2 Superresolution

Image superresolution techniques can be broadly categorized into interpolation-based methods, reconstruction-based methods and learning-based methods. The interpolation-based approach estimate the high-resolution image by assigning an intensity value to the unknown pixels based on the surrounding known pixels. The simplest among interpolation based approaches is bicubic interpolation [**48**]. This method does not exploit underlying structures in images, thus tends to blur the high-frequency details and introduce artifacts. Improved interpolation based approaches [**49**] [**50**] [**51**] consider latent structures during interpolation process, thus improving the SR quality. The reconstruction based approach [**52**] [**53**] [**54**] enforces a reconstruction constraint which

requires that the smoothed and down-sampled version of the HR image should be close to the LR image. Back-projection [**53**] is a most celebrated reconstruction based SR method. The major drawback of reconstruction-based SR approaches is a degraded performance for higher magnification factors.

Classical reconstruction based SR methods attempted to restore a high-resolution image by combining multiple low-resolution observations. Due to difficulty in obtaining image sequences for same LR image, new age methods use information from single low-resolution image to reconstruct HR image based on training sets. For this reason, learning based single-image super-resolution (SISR) methods have attracted more attention in recent years [**55**]. Learning-based approaches [**56**] [**57**] [**58**] [**59**] [**7**] embed more information into LR images from learning examples. These methods utilize this embedded information to model the relationship between the low-resolution and high-resolution image patches. The question still arises that how many training images are sufficient for the generic images.

2.2.1 Sparse Representation based Superresolution

Recently, sparse representation based learning methods [**6**] [**7**] [**55**] [**60**] [**61**] [**62**] [**63**] [**64**] [**65**] [**66**] has drawn considerable attention in the field of superresolution. This attention is based on the assumption that an image can be restored as a linear combination of atoms from an overcomplete dictionary. Sparse representation based techniques identify ingredients of the image, also referred as atoms and construct overcomplete dictionaries of these atoms. Now same or similar image can be reconstructed back using few atoms from the dictionary.

Yang *et al.* [**7**] presented a sparse coding-based superresolution framework, which learn coupled dictionaries from the training set of randomly sampled low and high-resolution image patches and then utilize sparse representations of the low-resolution image patch to generate the corresponding high-resolution image patch. The major problem in this method lies in deciding the total number of atoms in the coupled dictionary. Large numbers of atom increases the computation time of algorithm, however reducing the number of atoms degrades the super-resolution results remarkably. Zeyde *et al.* [**67**] succeeded in reducing the overall computational complexity of Yang's algorithm [**7**] by simplifying overall process. Zhu *et al.* [**68**] presented a self-example-learning-based sparse reconstruction approach to increase the computation speed. Instead of having external training set containing a large collection of HR images for dictionary learning, this method samples patches from the low-resolution input image itself. Rueda *et al.* [**61**] proposed SR approach specific to MR images that was a combination of image multi-scale edge analysis and a dimensionality reduction scheme for improvement in the SR reconstruction accuracy and computational speed. Lu *et al.* [**69**] also presented an SR algorithm specific to MR images, which exploits the local manifold structure of image patch pair, and applied locally linear embedding (LLE) regularizer into the traditional sparse coding framework. Tang *et al.* [**65**] suggested improvements in Yang's algorithm [**7**] by using flexible regression methods and L2-Boosting.

Further in the direction of accurate recovery of HR images Yang *et al.* [**62**] introduced the concept of examples-aided redundant dictionary learning. This method learns multiple compact dictionaries from the raw patches classified by K-means clustering. Yang *et al.* [**66**] proposed another method incorporating a Gaussian

neighbourhood based similarity regularizer term to exploit the non-local structural similarities of medical images. Liu *et al.* [**63**] applied the group sparse representation based SR approach to infrared surveillance. Recently Lu and Sun [**70**] proposed context-aware single image super-resolution method for reconstructing edge-preserving HR image. Kato *et al.* [**71**] experimented with the multi-frame approach in sparse coding-based image superresolution. Their main contribution was to handle a variable number of LR observations by the combination of sub-pixel accuracy block matching and LR atom generation from HR atoms. Motivated from multi-scale self-similarities in natural images Zhang *et al.* [**72**] proposed a structure-modulated sparse representation based SR method that combines multiple regularization prior i.e. structural self-similarity, the gradient histogram, and the nonlocal sparsity. In the present literature, there is a dearth of information related to sparse representation based fingerprint superresolution.

2.3 Fingerprint Enhancement

Fingerprint images are generally of low quality, because of the contexts of the image-acquisition process.Various methods [**23**] [**73**] [**74**] [**75**] [**76**] [**77**]have been suggested in literature to enhance the quality of fingerprint images. Fingerprint enhancement methods are roughly categorized into spatial and frequency domain. Yang *et al.* [**78**] proposed a two-stage method with the combination of spatial and frequency domain filters. For eliminating noise from fingerprint image variety of filters were proposed earlier such as contextual filters [**79**], Gabor filters [**73**] [**74**], anisotropic filters [**80**], image-scale-based filters [**81**] [**82**], directional filters [**23**] [**83**].

Although a lot of research has been conducted in past for enhancement of fingerprints to improve the performance of recognition process, but superresolution of

biometric images is still a gray area and needs the keen attention of researchers. The superresolution techniques can be incorporated into any traditional fingerprint enhancement for rendering better results [**84**] [**85**]. Better resolution enables the recognition algorithms based on minutiae detection or matching of ridge patterns to work more reliably and accurately. Specifically in crime investigation scenarios, superresolution of fingerprints can be very effective where acquired images are of very low resolution.

2.4 Contrast Enhancement

Poor contrast images do not occupy the complete dynamic range. Images having histogram bins concentrated toward a lower part or the darker grey levels possess low-intensity exposure whereas images having histogram bins concentrated toward a higher part, or the brighter part possess high-intensity exposure. Both types of images possess low contrast and need suitable contrast enhancing tools to improve the overall quality of an image. Histogram equalization based contrast enhancement technique is most popular and extensively utilized technique due to ease of implementation and its simplicity [**86**].

2.4.1 Histogram Equalization based Contrast Enhancement

Many histogram equalization based image enhancement methods were proposed to cope with contrast related issues. HE flattens the probability distribution and stretches the dynamic range of gray levels, which in result improves the overall contrast of the image. Applying HE straight away on natural images is not suitable for most consumer electronics applications, due to the problem of mean-shift i.e., the mean brightness of the output image and input image have a significant difference.

Kim proposed brightness preserving bi-histogram equalization (BBHE) [**87**] to preserve the mean image brightness. BBHE method first partitions the image's histogram into two sub-histograms based on the mean of the image's brightness and then histogram equalization process is performed on two sub-histograms independently. Wang *et al.* [**88**] proposed an algorithm named dualistic sub-image histogram equalization (DSIHE) which divides the image histogram based on median value i.e. each sub-histogram contains almost equal number of pixels and achieves good results in terms of detail preservation. Minimum mean brightness error bi-histogram equalization (MMBEBHE) [**89**] method perform the partition using the separating point that yields the minimum absolute mean brightness error (AMBE). Recursive mean-separate histogram equalization (RMSHE) [**90**] and recursive sub-image histogram equalization (RSIHE) [**91**] were proposed as recursive variants of BBHE and DSIHE. RMSHE and RSIHE methods have a challenging task of finding the optimal value of iteration factor (r) for producing efficient enhancement results. Kim and Chung [**92**] presented a method named Recursively Separated and Weighted Histogram Equalization (RSWHE) that modify the histogram by weighting process using normalized power law function. Clipped histogram based techniques [**93**] [**94**] [**95**] were proposed for controlling the over enhancement along with brightness preservation by histogram clipping.

Wadud *et. al.* [**96**] proposed dynamic histogram equalization (DHE) method that added a new dimension in histogram partitioning by dividing the image histogram based on local minima. The major drawback of this method is that it remaps the histogram peaks by allocating new dynamic range, which significantly changes the mean brightness.

Ibrahim and Kong **[**97**]**, proposed a variant of the DHE named as brightness preserving dynamic histogram equalization (BPDHE) and the partitioning criterion is local maxima. BPDHE also applies Gaussian-smoothing filter before the histogram sub-division process. Sheet et. al. **[**98**]** proposed a modification of the BPDHE technique named as Brightness Preserving Dynamic Fuzzy Histogram Equalization (BPFDHE). This method uses Fuzzy histogram computation for smoothing operation of histogram before partitioning of the image into sub-histograms. The authors of BPDFHE method proved the superiority of the algorithm in terms of less computational time and brightness preservation. These dynamic methods are suitable only for the images having significant peaks in the histograms.

Menotti *et al.* **[**99**]** proposed a Multi-Histogram equalization method to preserve the natural appearance of the image. Another method Dynamic Range Separate Histogram Equalization (DRSHE) **[**100**]** was proposed for preserving naturalness of an image, which separates the complete dynamic range into multiple parts and resizes the gray-scale range based on its area ratio. Quadrants dynamic histogram equalization (QDHE) **[**101**]** method is a hybrid approach where the histogram is partitioned into four sub-histograms. The partitioning criterion is the median value of intensity. In this method before assigning new dynamic range to each sub-histograms, the histogram clipping is performed based on the mean of the occupied intensity of the image. DQHEPL **[**102**]** is an extension of RSIHE method, computes four sub-histograms, and then assigns a new dynamic range to each sub-histogram and apply clipping process in the final step. Bi-Histogram equalization median plateau limit (BHEPLD) **[**102**]** is an extension of BHEPL, which applied the median value of intensity based criterion for clipping limit instead of the mean value of intensity occurrences.

Another variant of HE named as Brightness Preserving Weight Clustering Histogram Equalization (BPWCHE) **[**103**]** was introduced for simultaneously preserving the brightness of the image and enhancing visualization of the image. Simple Histogram Modification Scheme (SHMS) **[**104**]** algorithm is a histogram modification approach where the values of first and last boundary values of the support of histogram are changed. Although tremendous research has been conducted in the field of histogram equalization based contrast enhancement domain but still the potential of HE in solving the low-exposure imaging problem in less studied area.

2.5 Research Gaps

Based upon the analysis of earlier state-of-the-art methods on image quality improvement, following research gaps are identified:

- Fingerprint images often contain many repetitive geometric structures (or self-similarity) such as ridges and valleys; this self-similarity among patches has not been exploited in earlier research for better sparse representation.
- Considering the promising results of sparse representation based image denoising algorithms, addressing the fingerprint denoising with these algorithms is still less explored area.
- The process of image quality improvement through super-resolution methods is still a gray area in the field of fingerprint identification.
- In sparse representation based superresolution, self-similarity among patches in the form of repetitive geometric structures is less exploited.

- Poor contrast images do not occupy complete dynamic range. Natural images are often subject to low-exposure problems under low light or underwater conditions; contrast enhancement of low exposure images using histogram equalization is still a gray area.
- Although various techniques were proposed to cater specific problem of contrast enhancement, the problem of preservation of mean brightness, entropy, and control on the enhancement rate simultaneously is not addressed in earlier research.

2.6 Problems Addressed

The work presented in the thesis is mainly focused on design and development of reliable image quality improvement techniques. The answers to following questions are conveyed in this dissertation.

a) How do the repetitive geometric structures such as ridges and valleys in fingerprints can be exploited for better sparse representation of fingerprint images?
b) How can denoising and superresolution algorithms be incorporated in traditional enhancement methods to help in reliable and accurate fingerprint matching?
c) How can histogram equalization be effective in contrast enhancement of low exposure images?

In an attempt to answer these questions, we explored three dimensions of image quality improvement i.e. Denoising, Superresolution, and Contrast Enhancement.

2.7 Research Objectives

The major objective of this thesis is to propose novel image quality improvement techniques. Recent advancements in the field of sparse representation of images are the source of motivation behind formulating these research objectives. Based on the identified research problems in existing literature following objectives are formulated:

- Design of ridge orientation based clustered sparse dictionary learning algorithm to exploit self-similarity among patches for better sparse representation to increase the denoising and superresolution performance for the fingerprint.
- Design and development of sparse representation based fingerprint denoising algorithm.
- Design and development of sparse based fingerprint superresolution algorithm.
- Performance assessment of proposed fingerprint denoising and super-resolution method in terms of fingerprint recognition accuracy on standard public data sets.
- Development of contrast enhancement algorithm to address the problem of low exposure imaging
- Design and development of robust Histogram Equalization based contrast enhancement algorithm to cater problem of preservation of mean brightness, entropy and control on the enhancement rate simultaneously

CHAPTER 3
SPARSE REPRESENTATION BASED FINGERPRINT DENOISING

The problem of fingerprint denoising is peculiar in nature and need special methods for denoising. In this chapter, a novel framework for denoising fingerprint images is proposed. Instead of having a single sparse dictionary, the proposed method clusters the training patches into groups based on the dominant orientation of patch. Use of sub-dictionaries based on dominant orientation best describe the underlying image data and improves the effectiveness of sparse modeling of information in a fingerprint image in the form of local ridge patterns. Atoms from sub-dictionary with minimum residual error are used during reconstruction of patches. Denoising performance of proposed method is compared with other state-of-the-art denoising methods on public fingerprint databases.

3.1 Sparse Representation based Denoising Framework

The sparse based denoising framework comprises of restoring true image X from its noisy version Y contaminated with additive white Gaussian noise. The task involves suitable dictionary learning and coefficient calculation for efficient sparse representation of denoised image X. Elad and Aharon [**5**] proposed an image-denoising framework, which performs alternate minimization for learning patch-based dictionary where the size of each atom is equal to patch size. The energy minimization problem for image denoising boils down to

$$\{\hat{\alpha}, \hat{X}\} = \underset{\alpha_{i,j},X}{\operatorname{argmin}} \gamma\|X - Y\|_2^2 + \sum_{i,j}(\left\|\varphi\alpha_{i,j} - P_{i,j}(X)\right\|_2^2 + \ \beta\left\|\alpha_{i,j}\right\|_0 \ ) \quad (3.5)$$

where $P_{i,j}(X)$ is patch extraction operator. The above minimization process is a combination of three penalty terms; the first term imposes demand of proximity between the measured image, and its denoised counterpart. The second and third term demands that each reconstructed patch can be sparsely represented as linear combination of very few coefficients and dictionary with minimum error. The image denoising algorithm via energy minimization in Equation 3.5 involves an iterative block-coordinate relaxation method, which updates sparse coefficients, dictionary and image alternatively once at a time and keep other unknowns fixed.

3.2 Ridge Orientation Dictionary based Image Denoising

The proposed denoising algorithm comprises of three main steps: *Ridge orientation based clustering*, *Dictionary learning*, and *sparse coefficient calculation*.

3.2.1 Ridge Orientation based Clustering

A fingerprint is the pattern of ridges and valleys on the surface of the finger. Considering the fact that images especially fingerprint images often contains many repetitive geometric structures (or self-similarity) such as ridges and valleys, this self-similarity among patches is exploited here for better sparse representation, which in turn increases the denoising performance. The idea behind this approach is to group the patches containing similar geometric structures or dominant orientation and construct separate sub-dictionaries for each group. The orientation of ridge or a valley has been exploited in fingerprint matching algorithms [**105**] [**106**] in past. In the proposed method, the same concept of ridge orientation in the fingerprint to group the patches and to subdivide a

large dictionary into an array of sub-dictionaries is utilized. Ridge and valleys are main texture information embedded in fingerprint images and sparse modeling based on these features can significantly enhance the performance of sparse representation based denoising approach. Firstly, the patches are categorized into the smooth and rough patch by applying a variance threshold τ on each image patch. The rough patches are further classified into dominant and non-dominant orientation patches by applying a threshold on the dominant measure calculated by singular value decomposition (SVD) of the gradient vector of each patch. The estimation of local orientation is based on singular value decomposition (SVD) of the gradient vectors of the patch [**107**]. The method for this classification is described in following:

Calculate the local estimate of the gradient $\nabla y(u, v)$ at each i^{th} pixel at location (u, v) in the image patch.

$$\nabla y(u,v)_i = \left\{\frac{\partial I(u,v)}{\partial u}, \frac{\partial I(u,v)}{\partial v}\right\} \tag{3.6}$$

The gradient map $G \in R^{N\times 2}$ of the $\sqrt{p} \times \sqrt{p}$ patch is denoted as

$$G = \{\nabla y(u,v)_1, \nabla y(u,v)_2, \ldots\ldots, \nabla y(u,v)_p\}^T \tag{3.7}$$

Next step is to compute SVD of the gradient map

$$G = USV^T \tag{3.8}$$

Here $U \in R^{N\times N}$ represents each vector's contribution to the corresponding singular vector; $S \in R^{N\times 2}$ represent the energy in the dominant directions; and $V \in R^{2\times 2}$ represent the orientation, in which the columns v1 and v2 represents the dominant and subdominant orientation of the gradient field respectively. The categorization of rough patches into dominant or non-dominant orientation is decided based on a dominant measure R calculated as

$$R = \frac{S_1 - S_2}{S_1 + S_2} \tag{3.9}$$

where S_1 and S_2 are singular values representing the energy value in the dominant direction. The patches having dominant measure lesser than the significance level threshold R^* i.e. the singular values are remarkably different, it is very likely that the corresponding patch is only pure white noise and contains no dominant orientation [**107**]. The rough patches are categorized in dominant or non-dominant orientation patches for which the value of R is higher or lesser than significance level threshold R^* respectively.

The ridge orientation angle of all the dominant oriented patches is estimated by horizontal and vertical gradients of the patch. For finding ridge orientation angle of each patch, a gradient operator, is applied to obtain the horizontal gradient value G_r and vertical gradient value G_s and the block horizontal and vertical gradients i.e. G_{rr} and G_{rs} , are calculated by summing up all the pixel gradients of the particular direction.

$$G_{rs} = \sum_{u=i-\left(\frac{w}{2}\right)}^{i+\left(\frac{w}{2}\right)} \sum_{v=j-\left(\frac{w}{2}\right)}^{j+\left(\frac{w}{2}\right)} 2G_r(u,v)\, G_s(u,v) \tag{3.10}$$

$$G_{rr} = \sum_{u=i-\left(\frac{w}{2}\right)}^{i+\left(\frac{w}{2}\right)} \sum_{v=j-\left(\frac{w}{2}\right)}^{j+\left(\frac{w}{2}\right)} (G_r^2(u,v) - G_s^2(u,v)) \tag{3.11}$$

The most probable ridge orientation of the patch can now be obtained as

$$O(u,v) = \frac{1}{2}\tan^{-1}\left(\frac{G_{rs}}{G_{rr}}\right) \tag{3.12}$$

Once the ridge orientation of each dominant oriented patch is estimated further clustering is applied on the angles to group patches of similar structure in one cluster. For this algorithm, unsupervised classification technique, K-means clustering algorithm, which performs clustering of patches into some prefixed number of clusters is used. At the end of the clustering process, we have N clusters (classesΩ_n), one for smooth, and one for

non-dominant orientation patches and $N-2$ clusters for different ridge orientation angle patches.

3.2.2 Dictionary Learning

The image divided in overlapped patches of size $\sqrt{p} \times \sqrt{p}$ and each patch is ordered lexicographically as column vector $y_k \in R^p$; here k is the index of the patch. Next all the patches belonging to same sub-group are stacked in matrix denoted as $y_{\Omega_n} \in R^{p \times C_n}$ i.e. $y_{\Omega_n} = \{y_{\Omega_{n1}}, y_{\Omega_{n2}}, \ldots\ldots, y_{\Omega_{nC}}\}$, which consists of each patch represented by a column of the matrix. C_n is the number of patches in sub groups, and it may vary for different group. Once groups of patches of similar orientation are formed, next step is to train sub-dictionary for the individual group. The choice of dictionary φ is the heart of the sparse representation model.

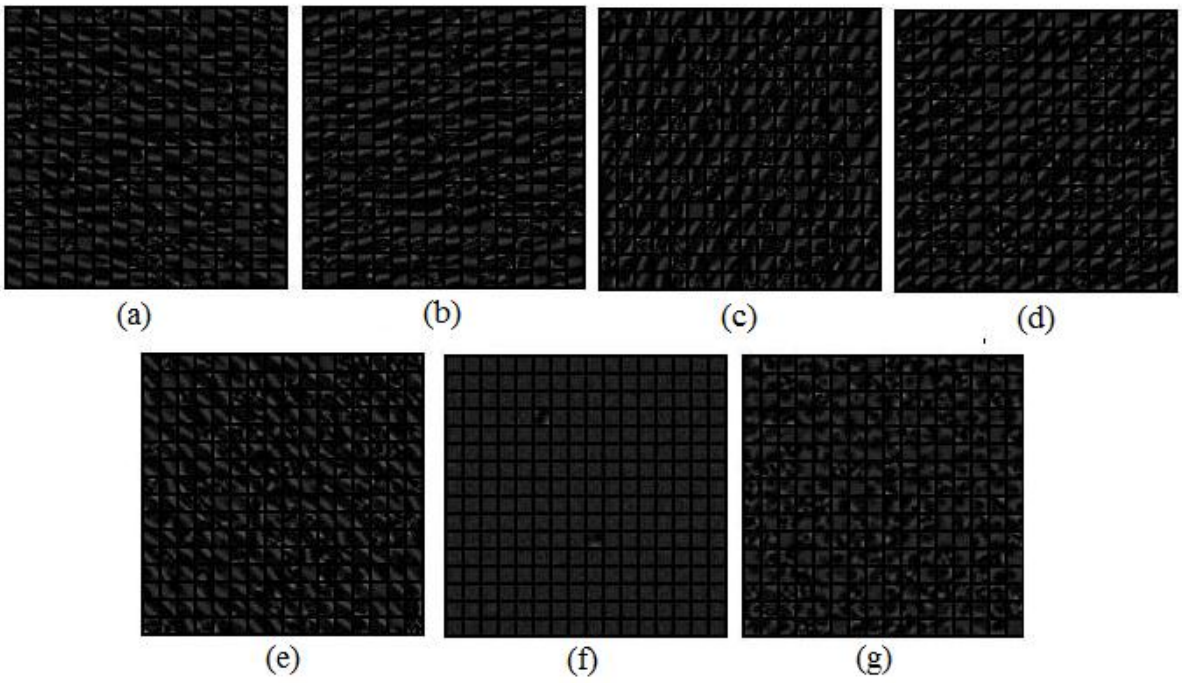

Figure 3.1 Ridge orientation based clustered sub-dictionaries (a) to (e) Dominant orientation (f). Smooth (g). Non-dominant orientation

The goal of dictionary learning is to optimize the dictionary and sparse coefficients jointly utilizing a set of given training image patches. The sub-dictionary training for each cluster can be formulated as

$$\{\hat{\alpha}_{\Omega_n}, \varphi^{(\Omega_n)}\} = \underset{\alpha,\varphi}{\operatorname{argmin}} \sum_{k\in\Omega_n} (\left\|\varphi^{(\Omega_n)}\alpha_{\Omega_n} - y_k\right\|_2^2 + \beta\left\|\alpha_{\Omega_n}\right\|_0) \quad (3.13)$$

where $n = 1,2,\ldots..N$ is the index of sub-dictionaries learned for each sub group of patches classified based on dominant orientation. K-SVD [**42**] is a natural choice for dictionary learning due to its simplicity and ease of implementation. In addition to it, the K-SVD dictionary learning process has in it a noise rejection capability [**5**]. The dictionary learning step yields N sub-dictionary $\{\varphi^{(\Omega_1)}, \varphi^{(\Omega_2)}, \ldots\ldots, \varphi^{(\Omega_N)}\}$ and the number of atoms are adaptive to the total number of patches in each group. For fingerprint images, the smooth and non-dominant orientation groups have less number of patches; hence, a lesser number of atoms can be allotted to corresponding sub-dictionary. Figure 3.1 shows typical sub-dictionaries learned based on ridge orientation based clustered patches.

3.2.3 Sparse Coefficient Calculation

Once the sub-dictionaries are learned for each cluster, the next step is to calculate the sparse coefficients to obtain the denoised image. Estimation of the sparse coefficients $\hat{\alpha}$, comes down to solve Equation 3.4. Orthogonal Matching Pursuit (OMP) algorithm is the best choice due to its speed and easy parameter tuning facility for solution of given optimization equation. Given the set of sub-dictionary $\{\varphi^{(\Omega_1)}, \varphi^{(\Omega_2)}, \ldots\ldots, \varphi^{(\Omega_N)}\}$ we form a sparse coefficient matrix for each patch corresponding to every sub-dictionary. The Equation 3.4 can be re-formulated as

$$\hat{\alpha}^{(\Omega_n)} = \underset{\alpha}{\operatorname{argmin}} \left\| y_k - \varphi^{(\Omega_n)} \alpha \right\|_2^2 + \beta \|\alpha\|_1 \tag{3.14}$$

Here $n = 1,2, \ldots . N$ is index for sub-dictionaries.

To recover the denoised patch for a given noisy patch, the sparse coefficients $\{\hat{\alpha}^{(\Omega_n)}\}$ are calculated using each of the sub-dictionaries and the residual error $\epsilon^{(\Omega_n)}$ is calculated by following equation for each dictionary

$$\left\{\epsilon^{(\Omega_n)}\right\} = \left\| y_k - \varphi^{(\Omega_n)} . \hat{\alpha}^{(\Omega_n)} \right\|_2 \tag{3.15}$$

The sub-dictionary having least residual error is chosen for that particular patch for reconstruction of the corresponding denoised patch. The final denoised image is obtained by aggregation of all estimated denoised patches $\{y_k\}$.

3.3 Experimental Results

To evaluate the performance of proposed method we have devised a validation methodology consisting of three experiments. In the first experiment, the proposed method is compared with NLM [**29**], K-SVD [**5**] and KLLD [**14**] methods in terms of quality measures i.e. PSNR and SSIM. Further, the proposed method is investigated in terms of visual quality. Authors believe that visual inspection and quality measures are not sufficient to evaluate the performance of fingerprint denoising. Filter bank based fingerprint matching [**105**] techniques have proved to be very effective in fingerprint matching. We have also used the same concept for performance evaluation and compared the Euclidean distance parameter of proposed method with other methods. Zero mean additive white Gaussian noise with different standard deviation was added in images to produce the noisy version. The effectiveness of the proposed method is evaluated on public databases FVC2000, FVC2002 and FVC2004. We have set empirical values of

variance threshold $\tau = 50$ and significance level threshold $R^* = 0.175$ for the classification of image patches into smooth, dominant or non-dominant orientation. These values can be manually fine-tuned as per requirement of the data set, taking higher or lower values of these parameters can result into the classification of smooth/non-dominant orientation patch into dominant orientation patch and vice versa. Total seven sub-dictionaries including one for smooth and one for non-dominant orientation are learned from the group of patches clustered on the basis of ridge orientation. Based on the distribution of patches in each group number of clusters is chosen. A higher number of clusters is not providing any significant improvement in results and sometimes results into very few patches in a sub group.

3.3.1 Comparison of Denoising Performance

For assessment of the performance of the algorithm, we have chosen two quality measures named as Peak Signal to Noise Ratio (PSNR) and Structural Similarity Index (SSIM).

PSNR is the ratio between the maximum possible power of a signal and the power of corrupting noise and expressed in terms of the logarithmic decibel scale. The PSNR is calculated as

$$PSNR = 10 \times \log \frac{255^2}{MSE};\ MSE = \frac{1}{MN}\sum_{m=0}^{M-1}\sum_{n=0}^{N-1}[\ A(m,n) - B(m,n)\ ]^2 \quad (3.16)$$

A is original image and B is the output of proposed method.

SSIM measures the structural similarity between the input and output images. SSIM depicts the distortion of the visual sensing. The SSIM is defined as

$$SSIM(a,b) = \frac{(2\mu_a\mu_b + c_1)(2\sigma_{ab} + c_2)}{(\mu_a^2 + \mu_b^2 + c_1)(\sigma_a^2 + \sigma_b^2 + c_2)} \quad (3.17)$$

where μ_a and μ_b are the mean values of images A and B, σ_a and σ_b are the standard deviation, σ_{ab} is the covariance, $c_1 = (K_1 L)^2$ and $c_2 = (K_2 L)^2$,with L being the maximum pixel value, K_1 = 0.01 and K_2 = 0.03) [**108**].

Observation noise with varying variance is added, and four typical values of sigma 10, 20, 30 and 40 are taken for experimentation. The PSNR values depicted in Table 3.1 clearly defines the superiority of proposed method over other methods. A dataset of 40 test images selected from three databases is constructed, and mean PSNR is calculated for all the methods and results are presented in Table 3.1 for analysis purpose. From the analysis of results, we now conclude that the proposed algorithm has achieved highly competitive PSNR performance for all the target images.

Table 3.1 *The PSNR results (in dB) of all algorithms for various noise levels*

Image	Sigma	Proposed Method	KSVD [5]	NLM [29]	KLLD [14]
Fingerprint 1	10	**31.6769**	30.9895	31.3191	30.8434
	20	**27.7703**	27.5687	27.1032	27.7517
	30	25.5703	**25.8326**	25.6037	24.5308
	40	**24.6637**	24.6077	24.2337	21.7344
Fingerprint 2	10	**30.4791**	30.2634	30.3297	29.9843
	20	**26.8613**	26.4305	26.5142	26.2517
	30	**24.6845**	24.6765	24.5067	24.4398
	40	23.5657	**23.7767**	23.4236	22.9374
Fingerprint 3	10	32.3242	32.0569	**32.5172**	32.1924
	20	**28.8809**	28.4793	28.6791	28.7545
	30	**26.7896**	26.6678	26.7243	26.6304
	40	25.2794	25.3067	**25.3372**	24.6609

Fingerprint 4	10	**31.7684**	31.4329	31.5460	30.9760
	20	**27.8767**	27.6472	27.7545	27.1518
	30	**25.7345**	25.6985	25.4057	25.2378
	40	24.5574	**24.5796**	24.3289	24.1384
Mean (40 Images)	10	**32.5621**	32.0856	32.3280	31.9990
	20	**26.8473**	26.4314	26.1127	26.0774
	30	**25.6947**	25.1188	25.5601	25.2097
	40	**23.5165**	23.3676	23.3308	22.3677

Similar to Table 3.1, mean SSIM is calculated on same the dataset and Table 3.2 depicts the SSIM performance results of proposed method in comparison with other three methods. From the comparative analysis, it is concluded that the proposed algorithm provides excellent SSIM performance for higher noise levels.

Table 3.2 *The SSIM results of all algorithms for various noise levels*

Image	**Sigma**	**Proposed Method**	**KSVD [5]**	**NLM [29]**	**KLLD [14]**
Fingerprint 1	10	**0.9210**	0.8807	0.8761	0.9035
	20	0.8337	0.8026	0.8126	**0.8594**
	30	**0.7856**	0.7690	0.7791	0.7674
	40	**0.7680**	0.7421	0.7537	0.6634
Fingerprint 2	10	**0.9323**	0.9007	0.9167	0.9129
	20	0.8554	**0.8664**	0.8517	0.8429
	30	**0.8119**	0.8097	0.8023	0.8009
	40	**0.7878**	0.7756	0.7796	0.7239
Fingerprint 3	10	**0.9192**	0.9118	0.9087	0.9034
	20	**0.8426**	0.8336	0.8419	0.8287
	30	**0.7998**	0.7726	0.7829	0.7817
	40	**0.7678**	0.7624	0.7569	0.7556

Fingerprint 4	10	0.8947	**0.8959**	0.8897	0.8761
	20	**0.8267**	0.8213	0.8179	0.8127
	30	**0.7786**	0.7623	0.7645	0.7527
	40	**0.7492**	0.7337	0.7423	0.7242
Mean (40 Images)	10	**0.9168**	0.8772	0.8678	0.8589
	20	**0.8396**	0.8209	0.8110	0.8059
	30	**0.7939**	0.7784	0.7822	0.7756
	40	**0.7682**	0.7434	0.75812	0.7167

3.3.2 Performance Assessment based on Fingerprint Matching

Euclidean distance parameter [**105**] is used here for evaluating the performance in terms of fingerprint matching. Results in Table 3.3 clearly indicate that proposed method is superior in terms of fingerprint matching. The Euclidean distance for proposed method is significantly less than other methods for most of the cases.

Table 3.3 *The Euclidean distance results of all algorithms for various noise levels*

Image	**Sigma**	**Proposed Method**	**KSVD [5]**	**NLM [29]**	**KLLD [14]**
Fingerprint 1	10	**20.3062**	22.3375	115.6792	26.5409
	20	**60.9436**	88.9767	98.7143	74.2789
	30	**91.1935**	129.8676	133.5734	98.5879
	40	**100.0349**	136.6567	126.5106	111.6721
Fingerprint 2	10	**32.3062**	36.8976	69.7865	33.2789
	20	87.8761	87.6678	98.8978	**86.2639**
	30	**102.3498**	103.5610	112.5678	121.7754
	40	**121.6123**	124.1245	123.2730	125.7699

Fingerprint 3	10	**26.7645**	29.3321	26.8961	27.8510
	20	**56.5643**	57.2331	59.0089	58.9002
	30	**80.0126**	82.2094	80.9429	83.2184
	40	**98.0197**	99.2970	100.5697	100.6573
Fingerprint 4	10	40.5692	**40.1297**	48.0371	40.3201
	20	**85.9709**	89.3264	86.2340	88.0362
	30	105.6931	109.3287	109.2367	**103.1017**
	40	**132.0289**	133.3079	138.4563	137.2843

3.3.3 Visual Performance Comparison

Figures 3.2 to 3.5 show the visual performance comparison of proposed method with KLLD, KSVD, and NLM method. It is important to emphasize that the visual impressions of resultant image of proposed method are very close to the original image.

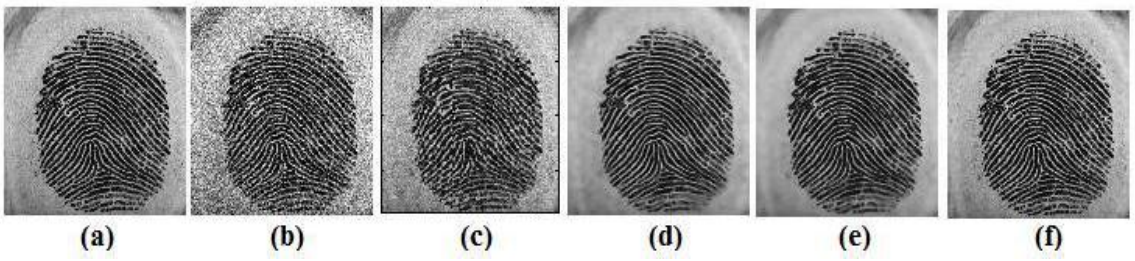

Figure 3.2 Visual performance comparison of different denoising methods (a). Original (b). Noisy (c). K-LLD (d). K-SVD (e). NLM (f). Our Method

The visual similarity is the key feature for fingerprint matching; therefore, it is an important aspect to be taken under consideration while performing image denoising of fingerprints. From the results, it is evident that KSVD and NLM methods have introduced distortion of blur in the fingerprints in figure 3.3 and 3.4; however, the KLLD results are also close to the original image but KLLD is not able to filter out the noise

completely. The visual results accord with the numerical results in terms of Euclidean distance.

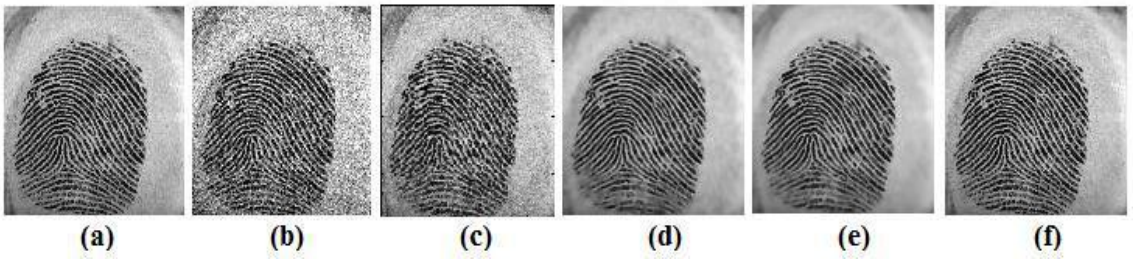

Figure 3.3 Visual performance comparison of different denoising methods (a). Original (b). Noisy (c). K-LLD (d). K-SVD (e). NLM (f). Our Method

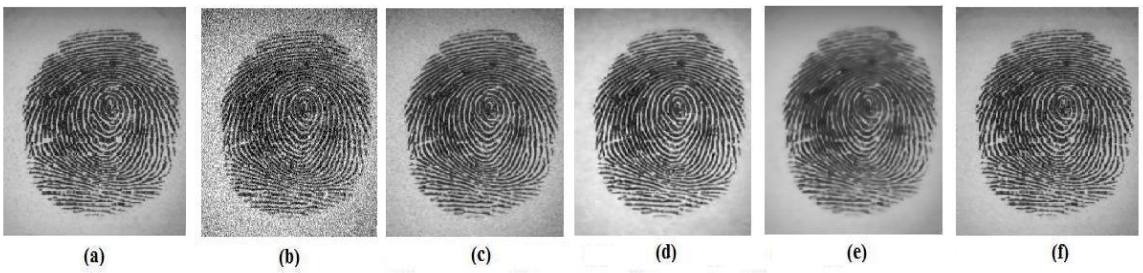

Figure 3.4 Visual performance comparison of different denoising methods (a). Original (b). Noisy (c). K-LLD (d). K-SVD (e). NLM (f). Our Method

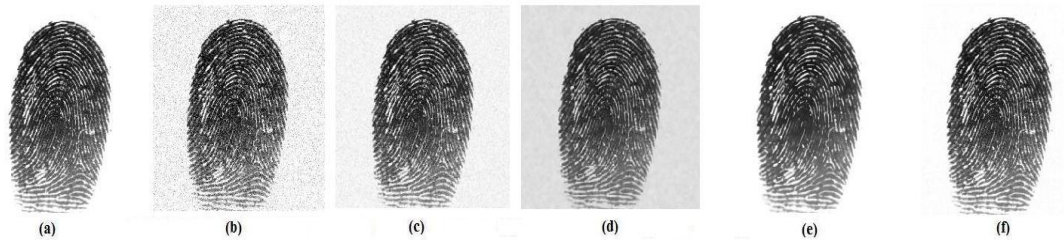

Figure 3.5 Visual performance comparison of different denoising methods (a). Original (b). Noisy (c). K-LLD (d). K-SVD (e). NLM (f). Our Method

3.4 Significant Findings

This chapter addressed the problem of fingerprint denoising. A novel approach of ridge orientation based sparse dictionary learning is proposed. The significant findings of the chapter are listed below

(a) Sub-dictionary trained for sub-groups formed of geometrically similar patches, work more effectively and this will help in improving denoising performance.

(b) Use of sub-dictionaries based on ridge orientation significantly improved the effectiveness of sparse modeling of information in a fingerprint image in the form local ridge patterns.

(c) The simulation results demonstrate that the new method achieves better results in comparison with its counterparts and will establish in improving performances of fingerprint-identification systems

This chapter is based on the following work:

***Kuldeep Singh**, Rajiv Kapoor, Raunaq Nayar, "Fingerprint denoising using ridge orientation based clustered dictionaries", Neurocomputing (**Elsevier, Impact factor-2.292**) 167(2015)418-423 (DOI:10.1016/j.neucom.2015.04.053)* [**109**]

CHAPTER 4

SPARSE REPRESENTATION BASED FINGERPRINT SUPERRESOLUTION

This chapter demonstrates a novel ridge orientation based sparse fingerprint superresolution algorithm. This approach is motivated by recent advancements in single image superresolution using sparse representation. The orientation of ridge or a valley has been exploited in fingerprint matching algorithms [**106**] [**105**] in past. In the proposed method, the same concept of dominant orientation has been utilized to subdivide a large dictionary into the array of sub-dictionaries to exploit self-similarity among patches. The training image patches are clustered into groups based on the orientation of ridge structures present in fingerprint images, and a sub-dictionary is learned for each cluster. While reconstructing HR patches, a suitable sub-dictionary is adaptively chosen by calculating residue error for each sub-dictionary. Back projection is further utilized to eliminate the discrepancy due to sparse modeling and noise.

4.1 Fingerprint Superresolution using Clustered Coupled Sparse Dictionaries

The proposed fingerprint superresolution algorithm comprises of three main steps: *Ridge orientation based clustering*, *Dictionary learning*, *Sparse superresolution*, *and Back projection.*

4.1.1 Ridge Orientation based Clustering

This method is very similar to that of explained in Section 3.1.1; however, it is explained here for better understanding of chapter. A fingerprint image consists of textured information. A small patch in a fingerprint image contains local structures such as ridges and valleys. Considering the fact that fingerprint images often contains many repetitive geometric structures (or self-similarity), we exploit this self-similarity among patches for better sparse representation, which in turn increases the superresolution performance. The idea behind this approach is to group the patches containing similar geometric structures or dominant orientation and construct separate sub-dictionaries for each group. The orientation of a ridge or a valley in the local patch has been exploited in fingerprint matching algorithms [**106**] [**105**]. In our experiment, we have utilized the same concept of local ridge orientation to subdivide a larger dictionary into array of sub-dictionaries for different orientation angles i.e. $D = \{D_1, D_2, D_3, \dots\dots\dots\dots\dots D_K\}$. Dividing the dictionary based on dominant orientation helps in improving the effectiveness of sparse modeling of information in a fingerprint image in form local ridge patterns. The sub-dictionaries are trained separately using training patches classified according to dominant orientation of ridges. Preprocessing step is carried out to separate out the patches not having any dominant orientation are classified as flat, and a separate sub-dictionary is constructed for those patches. The variance of gradient features is compared with a threshold value (σ_{th}) to obtain the above classification.

For finding gradient features of each patch, a gradient operator, is applied to obtain the horizontal gradient value G_x and vertical gradient value G_y. The block

horizontal and vertical gradients i.e. G_{xx} and G_{xy} , are calculated for dominant orientation patches by summing up all the pixel gradients of the particular direction .i.e.

$$G_{xy} = \sum_{u=i-(w/2)}^{i+(w/2)} \sum_{v=j-(w/2)}^{j+(w/2)} 2G_x(u,v)\, G_y(u,v) \tag{4.1}$$

$$G_{xx} = \sum_{u=i-\left(\frac{w}{2}\right)}^{i+\left(\frac{w}{2}\right)} \sum_{v=j-\left(\frac{w}{2}\right)}^{j+\left(\frac{w}{2}\right)} (G_x^2(u,v) - G_y^2(u,v)) \tag{4.2}$$

The most probable orientation of the patch can now be obtained as:

$$O(x,y) = \frac{1}{2}\tan^{-1}\left(\frac{G_{xy}}{G_{xx}}\right) \tag{4.3}$$

Once the ridge orientation of each patch is estimated further clustering is applied on the angles to group patches of similar structure in one cluster. For our algorithm, we run unsupervised classification technique, K-means clustering algorithm, which performs clustering of patches into some prefixed number of clusters. At the end of the clustering process, we have K clusters: $\{L\} = \{L_1, L_2, L_3, \ldots\ldots\ldots\ldots\ldots L_K\}$ (classesΩ_k), which includes one cluster for smooth patches.

4.1.2 Dictionary Learning

A separate coupled dictionary is trained for each cluster framed in above step to get K sub-dictionary $\{D^{(\Omega_1)}, D^{(\Omega_2)}, \ldots\ldots, D^{(\Omega_K)}\}$ where $\mathrm{D}^{(\Omega_\mathrm{i})} = \left\{\widetilde{D_{l(\Omega_\mathrm{i})}}\ D_{h(\Omega_\mathrm{i})}\right\}^T$. For Dictionary construction a training set, composed by some high-resolution images $\{X_j\}$ is taken. The corresponding low-resolution image set $\{Y_j\}$ is constructed by down-sampling, $\{X_j\}$ by a factor S. By using bicubic interpolator, an up-sampled set of images of expected high-resolution size is constructed.

The image divided in overlapped patches of size $\sqrt{n} \times \sqrt{n}$ and each patch is ordered lexicographically as column vector $y_k \in R^n$; here k is the index of the patch.

Next all the patches belonging to same sub group are stacked in matrix denoted as $y_{\Omega_i} \in R^{n \times C_i}$ i.e. $y_{\Omega_i} = \{y_{\Omega_{i1}}, y_{\Omega_{i2}}, \dots\dots, y_{\Omega_{iC_i}}\}$, similarly $x_{\Omega_i} = \{x_{\Omega_{i1}}, x_{\Omega_{i2}}, \dots\dots, x_{\Omega_{iC_i}}\}$, which consists of each patch represented as a column of the matrix. C_i is the number of patches in i^{th} subgroup. The number of patches may vary for different sub groups. Once groups of patches of similar orientation are formed, next step is to train sub-dictionary for the individual group. The core of the sparse representation modeling lies in the choice of dictionary D. Textures, sharp edges, and corners of image play a crucial role in visual quality improvement while performing image super-resolution [**17**]. For that reason the gradient operator G is chosen in dictionary learning phase in sync with the superresolution phase. Therefore, the gradient dictionary for one cluster $\widetilde{D_l} \in R^{4n \times N}$ for LR images is defined as

$$\widetilde{D_{l(\Omega_1)}} = G D_{l(\Omega_i)} \tag{4.4}$$

Constructing an overcomplete dictionary involves the solution of following optimization problem

$$D = \arg min_{D,\alpha} \ \|X - D\alpha\|_2^2 + \mu\|\alpha\|_1 \ s.t. \|D_i\|_2^2 \leq 1, i = 1,2, \dots\dots N \tag{4.5}$$

For couple dictionary [**55**] corresponding to one cluster,$D = \left\{\widetilde{D_l} \ D_h\right\}^T$, $X = \left\{G\{y_i\}, \{x_i\}\right\}^T$ and N is the number of columns in the dictionary. K-SVD [**42**] is a natural choice for dictionary learning due to its simplicity and ease of implementation. In addition to it, the K-SVD dictionary learning process has in it a noise rejection capability.

Algorithm 4.1: Ridge Orientation based Dictionary Learning
Input: Training set of HR images

Step1. Generate LR training set by down sampling HR images and then interpolating them back to the size of expected super-resolved output image using bicubic interpolation.

Step2. Take patches of size $\sqrt{n}\ X\ \sqrt{n}$ from HR training set image $\{x_i\}$, $x_i \in R^{n\times 1}$ and gradient of LR training set $\{Gy_i\}$, $Gy_i \in R^{4n\times 1}$

Step3. Calculate the variance of each patch and classify flat patches based on the threshold value.

Step4. Compute ridge orientation for all patches using Equation (4.1) - (4.3)

Step5. Cluster the orientation angles of patches into K-1 sets by K- mean clustering.

Step6. Train coupled dictionary for each cluster using KSVD algorithm

For k= 1 to K

$$\{D_{hk}, \widetilde{D_{lk}}\} = KSVD(\{x_k, Gy_k\})$$

end

Output: Coupled dictionary $D = \{D_{hk}, \widetilde{D_{lk}}\}$; k = 1 to K $D_{hk} \in R^{n\times 200}$ *and* $\widetilde{D_{lk}} \in R^{4n\times 200}$

The K-SVD algorithm iteratively optimizes the above objective function and yields the coupled dictionary. The dictionary learning step yields K sub-dictionaries $\{D^{(\Omega_1)}, D^{(\Omega_2)}, \ldots\ldots, D^{(\Omega_K)}\}$ and numbers of atoms are adaptive to the total number of

patches in each group. For fingerprint images, the smooth groups have less number of patches; hence, lesser number of atoms can be allotted to corresponding sub-dictionary.

4.1.3 Sparse Superresolution

Once the coupled sub-dictionaries are learned for each cluster, the next step is to calculate the sparse coefficients for individual LR patches using the LR dictionary. For estimation of the sparse coefficients $\hat{\alpha}$, Orthogonal Matching Pursuit (OMP) algorithm is the best choice due to its speed and easy parameter tuning facility for the solution of given optimization equation. Given the set of LR sub-dictionary $\{\widetilde{D_{l(\Omega_1)}}, \widetilde{D_{l(\Omega_2)}}, \ldots\ldots\ldots \widetilde{D_{l(\Omega_K)}}\}$ we form a sparse coefficient matrix for each patch corresponding to every sub-dictionary. The problem of coefficient estimation can be formulated as

$$\hat{\alpha}^{(\Omega_n)} = \underset{\alpha}{\operatorname{argmin}} \left\| Gy_k - \widetilde{D_{l(\Omega_n)}}.\alpha \right\|_2^2 + \beta \|\alpha\|_1 \tag{4.6}$$

Here $n = 1,2, \ldots\ldots K$ is index for sub-dictionaries.

To recover an HR patch for a given LR patch, the sparse coefficients $\{\hat{\alpha}^{(\Omega_n)}\}$ are calculated using each of the sub-dictionaries and the residue error $\epsilon^{(\Omega_n)}$ is calculated by the following equation for each sub-dictionary

$$\left\{\epsilon^{(\Omega_n)}\right\} = \left\| Gy_k - \widetilde{D_{l(\Omega_n)}}.\hat{\alpha}^{(\Omega_n)} \right\|_2 \tag{4.7}$$

The sub-dictionary having least residue error is chosen for that particular patch for reconstruction of corresponding HR patch. The corresponding HR patch can be restored as

$$\widehat{x_k} = D_{h(\Omega_n)}.\hat{\alpha}^{(\Omega_n)} \tag{4.8}$$

The flat sub-dictionary classified earlier is used for reconstruction of HR flat patch. The final super-resolved image is obtained by aggregation of all estimated HR patches $\{x_k\}$.

4.1.4 Back Projection

For enhancing the superresolution performance and to preserve subtle details of the image, we enforce an iterative back projection mechanism that compensates the error. Suppose Y is original LR image and $\hat{X}$ is super-resolved image output of sparse superresolution step, now the $\hat{X}$ is down sampled *i.e.* $\hat{Y} = \psi\hat{X}$. Then we calculate the residual error $\varepsilon_r = Y - \hat{Y} = Y - \psi\hat{X}$. We apply the same proposed sparse superresolution algorithm on the residual error to find the HR version of residual error $\widehat{\varepsilon_r}$, the process can be defined as $\varepsilon_r = \psi\widehat{\varepsilon_r}$. Finally, high-resolution residual error $\widehat{\varepsilon_r}$ is added to the restored HR image to yield final estimate of latent image $X_{final} = \hat{X} + \widehat{\varepsilon_r}$.

Algorithm 4.2: Fingerprint Superresolution using Sparse Coding

Input: Coupled Dictionary $D = \{D_k\}; k = 1\ to\ K$, where $D_k = \{D_{hk}, \widetilde{D_{lk}}\}$ $D_{hk} \in R^{n\times 200}$, $D_{lk} \in R^{4n\times 200}$, a low-resolution image Y .

Step1. Repeat the following steps for all the patches of input image

1.1 Take $\sqrt{n}\ X\ \sqrt{n}$ size patch y_i of Y, with two overlapping pixels and Compute the mean pixel value m of patch y_i.

1.2 Compute first and second order gradient features to obtain Gy_i.

1.3 **For** k =1 to K (K number of sub-dictionaries)

Solve the optimization problem with $\widetilde{D_l}$ and Gy_i and find residue error r_k

$$min_{\alpha} \left\| \widetilde{D_{lk}} \alpha_k - G y_i \right\|_2^2 + \mu \|\alpha_k\|_1$$

$$r_k = \left\| G y_i - \widetilde{D_{lk}} . \alpha_k \right\|_2$$

end

1.4 Find the dictionary with minimum residue error $j = min_k(r_k)$

1.5 Generate the high-resolution patch $\hat{x_i} = D_{hj} . \alpha_j$

1.6 Add mean value $x_i^* = \hat{x_i} + m_i$

End

Step2. Regenerate HR image $\hat{X}$ by aggregation of HR patches $\{x_i^*\}$

Step3. Apply back projection on $\hat{X}$ for upto 5 iteration

Output: Superresolution image X_{final}.

4.1.5 Experimental Results

To demonstrate the performance of proposed method we have devised a validation methodology consisting three tasks. Firstly, the proposed method is compared with bicubic interpolation method [**48**], Yang's method [**7**] and Freeman's method [**57**] in terms of quality measures i.e. PSNR and SSIM. Then the proposed method is investigated in terms of visual quality. Authors believe that visual inspection and quality measures are not sufficient to evaluate the performance of fingerprint super-resolution. Filter bank based fingerprint matching [**105**] technique has proved to be very effective technique in

fingerprint matching hence we have also used the same concept for performance evaluation in terms of matching accuracy of proposed method with other methods.

4.1.6 Dataset and Simulation Details

The performance of the proposed method is evaluated on public databases FVC2000, FVC2002 and FVC2004. The images in the database are down sampled to constitute the LR set for training as well as test images for superresolution. The fingerprint images are randomly selected from all the 12 databases (4 databases each in FVC2000, FVC2002 and FVC2004) for training and evaluation. Results for scaling factor (SF) three and four are presented. Around 50000 image patches are sampled to train the coupled dictionaries, and the patches are clustered into six groups including one group for flat patches and five groups based on the dominant orientation of patch. The number of clusters is taken based on the distribution of patches in each group. Based on the distribution of patches in each group, the number of clusters is chosen. A higher number of clusters is not providing any significant improvement in results and sometimes results into very few patches in a group.

Table 4.1 *Centroids of Orientation angle clusters*

Cluster No	1	2	3	4	5
Centroid angle (degrees)	-74.1293	-47.148	2.0455	44.7824	75.0747

Table 4.1 shows the centroid value of orientation angle for each cluster computed using the K-mean algorithm. For each cluster dictionary of 200 atoms are trained. The variance threshold taken for separating the flat patches is $\sigma_{th} = 0.003$. This value can be manually

fine-tuned as per requirement of the data set. Taking higher or lower values of this parameter can result into the classification of the patch into dominant orientation patch and vice versa.

For reconstruction of the HR image, patches of size 9×9 (SF=3) and 11×11 (SF=4) were taken with overlapping of two pixels between adjacent patches to maintain the continuity. In our experiment, we found 10 iterations of the LARS/Lasso algorithm to be sufficient to give visually pleasing results. Increasing the number of iterations beyond a certain point does not lead to any improvement in the result but rather the sparsity of the solution i.e. $\|\alpha\|_1$ gets penalized to minimize the residue $\left\|\widetilde{D_{ll}}\alpha_i - G.y_i\right\|_2^2$, which leads to unnatural output HR image. After that the obtained HR image $\hat{X}$ is fine-tuned by back projection for up to five iterations. Gaussian filter with $\sigma = 1.5$ is also applied in back projection step to eliminate noise.

4.1.7 Performance Assessment based on Quantitative Performance Measures

For assessment of performance of the algorithm, we have chosen two quality measures named as Peak Signal to Noise Ratio (PSNR) and Structural Similarity Index (SSIM) [**108**]. Table 4.2 and 4.3 depict the PSNR values computed for various methods and proposed method has higher PSNR values in comparison to other methods especially for a higher scaling factor of four. It is also evident that back projection helps in improving the PSNR measure.

Table 4.2 *The PSNR (dB) of reconstructed image by different methods for SF=3*

Image	**Bicubic** [**48**]	**Yang *et al.*** [7]	**Freeman *et al.*** [57]	**Proposed method without back projection**	**Proposed method with back projection**

Fingerprint1	20.7040	22.3151	20.4756	20.6401	**22.6510**
Fingerprint2	18.9056	19.4280	18.3109	18.5615	**19.5281**
Fingerprint3	20.2412	20.1977	19.2135	19.6374	**20.8126**
Fingerprint4	25.2408	24.8742	23.5401	23.0860	**25.4709**
Fingerprint5	20.5495	22.1194	20.8496	20.6637	**23.0924**
Fingerprint6	19.8966	22.3512	20.4238	20.5230	**22.9931**
Mean (50 Images)	20.8247	21.0349	20.8968	20.9768	**22.1869**

Table 4.3 *The PSNR (dB) of reconstructed image by different methods for SF=4*

Image	**Bicubic** [**48**]	**Yang *et al.*** [**7**]	**Freeman *et al.*** [**57**]	**Proposed method without back projection**	**Proposed method with back projection**
Fingerprint1	20.3446	21.6845	20.2956	20.5147	**22.1582**
Fingerprint2	18.5363	19.3705	18.0118	18.1055	**19.3793**
Fingerprint3	19.8424	20.6765	19.0978	19.2804	**20.6995**
Fingerprint4	24.6913	25.0880	23.2395	23.0149	**25.1248**
Fingerprint5	20.2012	22.5300	20.4756	20.4854	**22.8605**
Fingerprint6	19.5344	21.6987	20.2983	20.3708	**22.2079**
Mean (50 Images)	20.5693	21.0049	20.4971	20.7382	**21.9754**

Table 4.4 *The SSIM of reconstructed image by different methods for SF=3*

Image	**Bicubic** [**48**]	**Yang *et al.*** [**7**]	**Freeman *et al.*** [**57**]	**Proposed method without back projection**	**Proposed method with back projection**
Fingerprint1	0.7064	0.7749	0.7377	0.7495	**0.7831**
Fingerprint2	0.6332	0.7069	0.6772	0.6775	**0.7093**
Fingerprint3	0.6992	0.7709	0.7291	0.7350	**0.7732**
Fingerprint4	0.6692	**0.7279**	0.6875	0.6923	0.7199
Fingerprint5	0.7499	0.8120	0.7721	0.7874	**0.8150**
Fingerprint6	0.7290	0.8105	0.7913	0.7939	**0.8270**
Mean (50 Images)	0.6868	0.7589	0.7198	0.7257	**0.7698**

Table 4.5 *The SSIM of reconstructed image by different methods for SF=4*

Image	**Bicubic** [**48**]	**Yang *et al.*** [**7**]	**Freeman *et al.*** [**57**]	**Proposed method without back projection**	**Proposed method with back projection**
Fingerprint1	0.6319	0.6880	0.6517	0.6509	**0.7123**
Fingerprint2	0.5643	0.6360	0.5620	0.5687	**0.6500**
Fingerprint3	0.6221	0.6907	0.6277	0.6288	**0.6975**
Fingerprint4	0.6027	0.6517	0.5916	0.5905	**0.6588**
Fingerprint5	0.6785	0.7425	0.6924	0.6986	**0.7504**
Fingerprint6	0.6605	0.7369	0.6995	0.7017	**0.7543**
Mean (50 Images)	0.6189	0.6810	0.6192	0.6278	**0.7021**

Tables 4.4 and 4.5 show the results of SSIM measure, which judges the structural similarity between the original and reconstructed image. Proposed method with or without back projection yields higher SSIM value that implies that the method preserves the structural aspects while super resolving the image.

Also, as seen with PSNR measure, SSIM values are much better than Yang's method for scaling factor four. It can be observed that quality of superresolution is better preserved with our method while Yang's method deteriorates when the higher scaling factor is required.

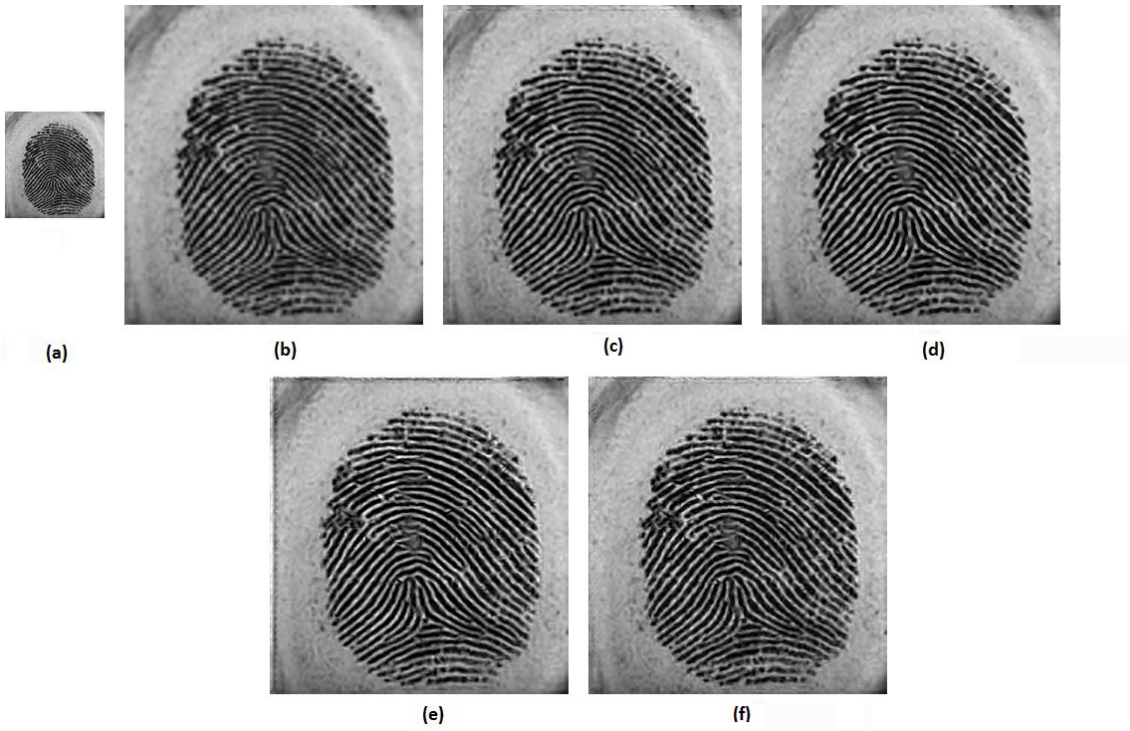

Figure 4.1 Visual performance comparison of different superresolution methods for Fingerprint1 (SF=3) (a) Original low resolution, (b) Bicubic, (c) Yang et al. , (d) Freeman et al., (e) Proposed method without back projection, (f) With back projection

A dataset of 50 test fingerprint images randomly selected from the databases is constructed and mean PSNR and mean SSIM is calculated for all the methods and results

are presented in Table 4.2-4.5 for analysis purpose. From the analysis of results, we now conclude that the proposed algorithm has achieved highly competitive PSNR and SSIM performance for all the target images.

4.1.8 Performance Assessment based on Visual Inspection

This subsection evaluates the performance of our algorithm in visual perspective. In figures 4.1-4.4, the low-resolution test image and the super-resolution images reconstructed by different super-resolution algorithms are depicted for super-resolution factor 3 and 4. Images taken here for visual inspection are of different contrast to test the robustness of the method.

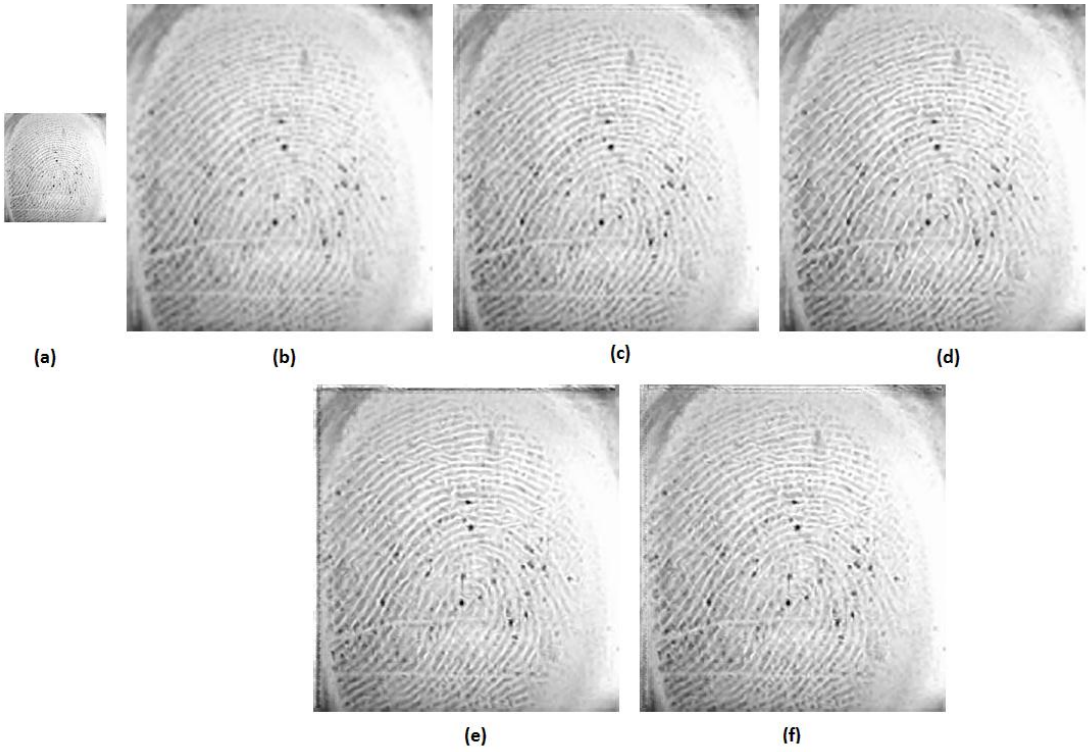

Figure 4.2 Visual performance comparison of different superresolution methods for Fingerprint2 (SF=3) (a) Original low resolution, (b) Bicubic, (c) Yang et al. ,(d) Freeman et al. , (e) Proposed method without back projection, (f) With back projection

Original image in Figure 4.1 and 4.3 is of higher contrast and results show that Bicubic and Yang's image are blurred in appearance, however; our method has produced blur-free image. Results in Figure 4.2 and 4.4 shows that proposed method is also well suited for fingerprint images of low contrast with light thumb impression and better in terms of information preservation. In fact, all the results show that our algorithm reconstructs images with the balance between the high-resolution details and the artifacts. From visual inspection, it is being observed that the resultant image with back projection is visually closer to the original image. However, from the result of image Fingerprint2 it is evident that back projection does not always lead to a better result.

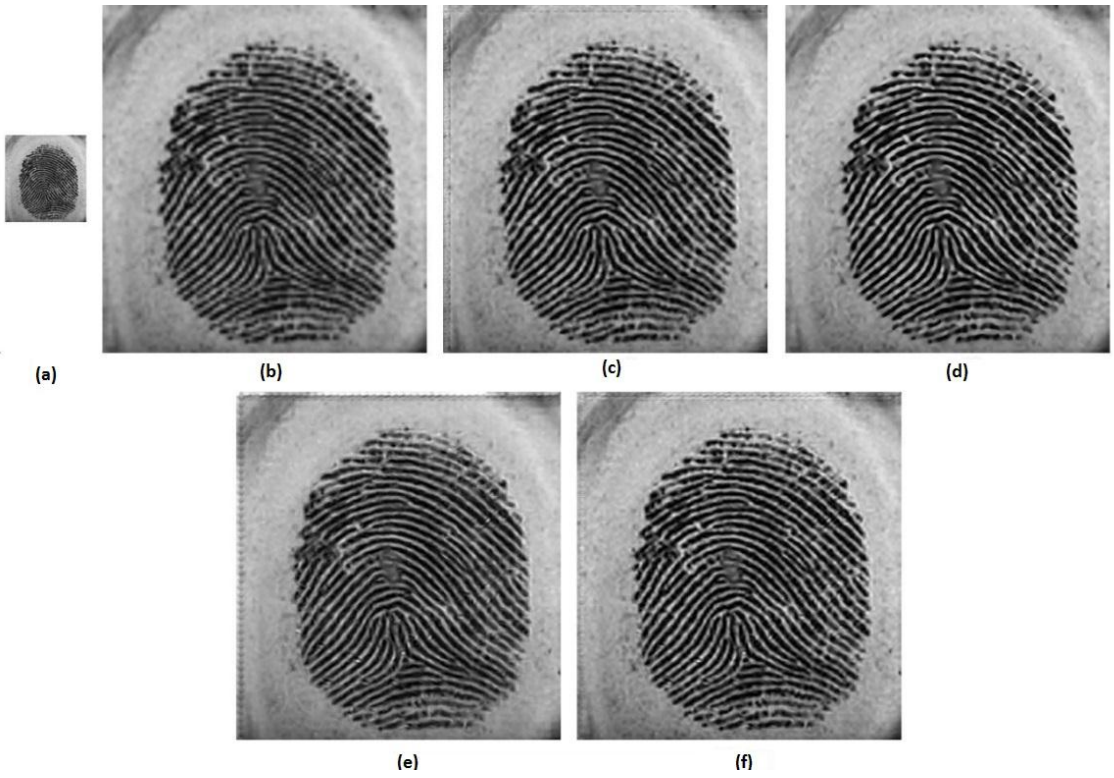

Figure 4.3 Visual performance comparison of different superresolution methods for Fingerprint1 (SF=4) (a) Original low resolution, (b) Bicubic, (c) Yang et al. ,(d) Freeman et al. , (e) Proposed method without back projection, (f) With back projection

4.1.9 Performance Assessment based on Fingerprint Matching

PSNR and SSIM measures are not sufficient to measure the performance for fingerprint superresolution. Filter-bank based fingerprint matcher [**105**] is used for evaluating the performance of proposed method in terms of matching accuracy. We evaluate the algorithms on a set of 800 images (100 users, 8 images each) derived from FVC2002 DB1 database.

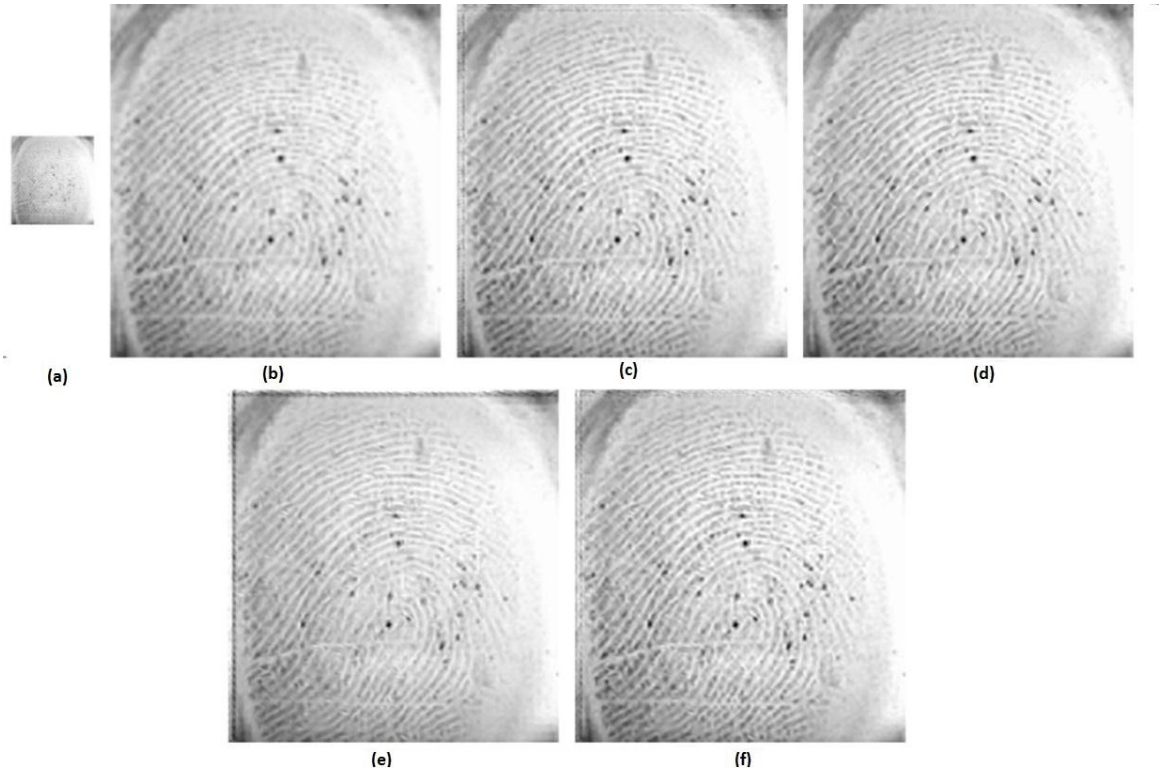

Figure 4.4 Visual performance comparison of different superresolution methods for Fingerprint2 (SF=4) (a) Original low resolution, (b) Bicubic, (c) Yang et al. ,(d) Freeman et al. , (e) Proposed method without back projection, (f) With back projection

For genuine attempts, each fingerprint impression is matched with the remaining impressions of the same finger and for imposter attempts the first impression of each finger is matched against the first impression of the remaining fingers. The total number of genuine and impostor comparison are 2800 and 4950, respectively.

The performance of proposed method is evaluated in terms of Equal error rate (EER) and Detection error tradeoff (DET) curve. EER is a threshold-independent performance measure calculated as an average of the total errors when FAR equals FRR. Better fingerprint matching systems have lower EER value. Figure 4.5 shows the DET curve of bicubic, Freeman *et al.*, Yang *et al.* and proposed method with the back projection for scaling factor four.

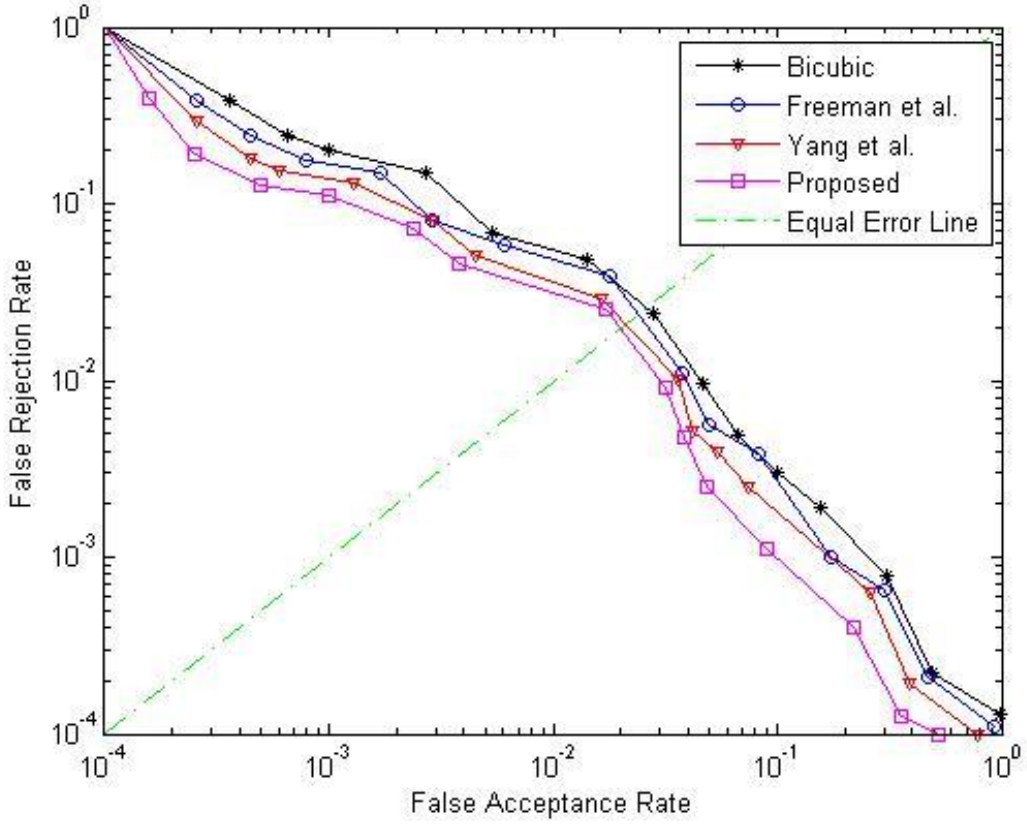

Figure 4.5. DET curve for different superresolution methods

As per the EER results depicted in Table 4.6 the proposed algorithm has lowest EER value. From the matching results, we can conclude that the proposed fingerprint superresolution algorithm has the best performance among other methods taken for comparison in terms of matching accuracy.

Table 4.6 *EER Results of different Superresolution Methods*

Methods	Bicubic [**48**]	Freeman *et al.* [**57**]	Yang *et al.* [**7**]	Proposed
EER(%)	3.12	2.53	1.92	**1.84**

4.2 Significant Findings

This chapter addressed the problem of fingerprint superresolution using ridge orientation based clustered coupled sparse dictionaries. The significant findings of the chapter are listed below

a) Use of sub-dictionaries based on dominant orientation (self-similarity) improved the effectiveness of sparse modeling of information in a fingerprint image in the form of local ridge patterns.
b) The inclusion of sub-dictionary for flat patches improved the reconstruction where dominant ridge orientation is not present.
c) Adaptive selection of suitable sub-dictionary while reconstruction based on minimum residue error criterion enhanced the performance of the algorithm.
d) Use of back projection method eliminated discrepancy due to noise or inaccuracy in the sparse representation.

This chapter is based on the following work:

Kuldeep Singh, *Anubhav Gupta , Rajiv Kapoor, "Fingerprint image super-resolution via ridge orientation based clustered coupled sparse dictionaries", Journal of electronic imaging (**SPIE, Impact factor- 0.832**) 20(4) (2015) (DOI:10.1117/1.JEI.24.4.043015)* [**110**]

CHAPTER 5

CONTRAST ENHANCEMENT USING HISTOGRAM EQUALIZATION

This chapter explains three novel proposed histogram equalization based contrast enhancement methods. The MMSICHE [**111**] method caters the problem of preservation of mean brightness, entropy and control over enhancement rate simultaneously. For contrast enhancement of low light images, Exposure based sub-image histogram equalization (ESIHE) [**112**] and two variants of ESIHE i.e. RESIHE and RS-ESIHE [**113**] are proposed. Detailed performance analysis of proposed methods is presented in terms of image quality measures as well as in terms of visual quality.

5.1 Median-Mean based Sub-Image Clipped Histogram Equalization

This method achieves multi-objective of preserving brightness as well as image information content (entropy) along with control over enhancement rate, which in turn suits for consumer electronics applications. This method avoids excessive enhancement and produces images with natural enhancement. The algorithm consists of three steps, namely Median and Mean calculation, Histogram clipping and Histogram subdivision & equalization. Following subsections present description of each step of the algorithm.

5.1.1 Median and Mean Calculation

The median of the image is denoted as an intensity value $X_e$where the cumulative density function is 0.5. Two mean intensity values (X_{ml} & X_{mu}) are calculated for two individual sub-histogram divided based on median value. The values of X_e, X_{ml} and $X_{mu}$are calculated before histogram clipping process. Equation 5.1 computes the total number of samples N for a given image

$$N = \sum_{k=0}^{L-1} h(k) \tag{5.1}$$

$h(k)$is the histogram of the image and L is the total number of gray levels. For calculating X_e consider a variable $z(k)$

$$z(k) = z(k-1) + h(k) \quad \text{for k} = 0,1 \ldots, \text{L} - 1 \ \& \ \text{z}(0) = \text{h}(0) \tag{5.2}$$

Median variable can be calculated as

$$X_e = k \; where \; z(k) \geq N/2 \tag{5.3}$$

Mean variables X_{ml} and X_{mu} are expressed as

$$X_{ml} = \sum_{k=0}^{X_e-1} P_l(k) \times k \tag{5.4}$$

$$X_{mu} = \sum_{X_e}^{L-1} P_u(k) \times k \tag{5.5}$$

where $P_l(k)$and $P_u(k)$are individual PDF the sub-histograms. Calculation of these PDFs is depicted below

$$P_l(k) = {}^{h(k)}/_{N_l} \; for \; k = 0,1, \ldots \ldots, X_e - 1 \tag{5.6}$$

$$P_u(k) = {}^{h(k)}/_{N_u} \; for \; k = X_e, X_e + 1, \ldots, L - 1 \tag{5.7}$$

N_l and $N_u$are total numbers of pixels in the lower and upper sub-histogram respectively.

5.1.2 Histogram Clipping

The idea behind the Histogram clipping is to control the enhancement rate consequently to result in a natural appearance of the image. For limiting the enhancement rate, we need to limit the first derivative of the histogram or the histogram itself [**95**].

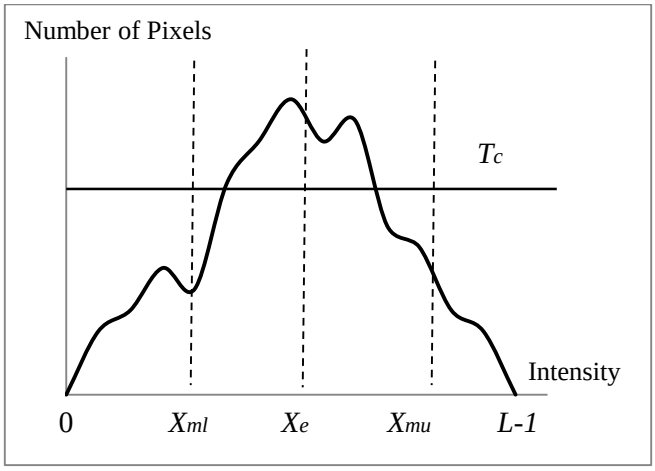

Figure 5.1 MMSICHE: Process of histogram clipping and sub division

The histogram bins having the value greater than the clipping threshold are limited to the threshold. The clipping threshold is calculated as the median of occupied intensity. The clipping threshold T_c and the clipped histogram is calculated as

$$T_c = median[h(k)] \tag{5.8}$$

$$h_c(k) = \begin{cases} h(k), & h(k) < T_c \\ T_c, & h(k) \geq T_c \end{cases} \tag{5.9}$$

$h(k)$and $h_c(k)$ are the original and clipped histogram. This method is computationally efficient and less time consuming. The clipping process is graphically illustrated in Figure 5.1.

5.1.3 Histogram Sub Division and Equalization

The original histogram is first bisected based on median intensity value X_e. These individual sub-histograms are further divided into two small sub-histograms where the individual mean X_{ml} and X_{mu} acts as a separating point of sub-histograms. The histogram sub division process results in four sub-images W_{Ll}, W_{Lu}, W_{Ul}, and W_{Uu}ranging from gray level 0 to X_{ml}, $X_{ml}+1$ to X_e, X_e+1 to $X_{mu}$and $X_{mu}+1$to *L-1*. $P_{Ll}(k)$, $P_{Lu}(k)$, $P_{Ul}(k)$ and $P_{Uu}(k)$are corresponding PDF of these sub-images.

$$P_{Ll}(k) = {h_c(k)}/{N_{Ll}} \; for \; 0 \leq k \; \leq X_{ml} \tag{5.10}$$

$$P_{Lu}(k) = {h_c(k)}/{N_{Lu}} \; for \; X_{ml}+1 \leq k \; \leq X_e \tag{5.11}$$

$$P_{Ul}(k) = {h_c(k)}/{N_{Ul}} \; for \; X_e+1 \leq k \; \leq X_{mu} \tag{5.12}$$

$$P_{Uu}(k) = {h_c(k)}/{N_{Uu}} \; for \; X_{mu}+1 \leq k \; \leq L-1 \tag{5.13}$$

N_{Ll}, N_{Lu}, N_{Ul} and $N_{Uu}$are total number of pixels in sub-images W_{Ll}, W_{Lu}, W_{Ul} and W_{Uu}respectively. C_{Ll}, C_{Lu}, C_{Ul} and C_{Uu} are corresponding CDF of individual sub-images as defined below

$$C_{Ll}(k) = \sum_{k=0}^{X_{ml}} P_{Ll}(k) \tag{5.14}$$

$$C_{Lu}(k) = \sum_{k=X_{ml}+1}^{X_e} P_{Lu}(k) \tag{5.15}$$

$$C_{Ul}(k) = \sum_{k=X_e+1}^{X_{mu}} P_{Ul}(k) \tag{5.16}$$

$$C_{Uu}(k) = \sum_{k=X_{mu}+1}^{L-1} P_{Uu}(k) \tag{5.17}$$

The next step of MMSICHE is to equalize all the four sub-histograms individually. The transfer functions for histogram equalization can be defined as below

$$F_{Ll} = X_{ml} \times C_{Ll} \tag{5.18}$$

$$F_{Lu} = (X_{ml} + 1) + (X_e - X_{ml} + 1) \times C_{Lu} \tag{5.19}$$

$$F_{Ul} = (X_e + 1) + (X_{mu} - X_e + 1) \times C_{Ul} \tag{5.20}$$

$$F_{Uu} = (X_{mu} + 1) + (L - X_{mu} + 1) \times C_{Uu} \tag{5.21}$$

F_{Ll}, F_{Lu}, F_{Ul} and $F_{Uu}$are the transfer functions used for equalizing the sub-histograms individually. The final step involves the integration of all sub-images into one complete image for analysis. The MMSICHE-ed output image is produced by the combination of all four transfer functions.

5.1.4 Simulation Results of MMSIHE Method

The simulation results of proposed MMSICHE method are compared with existing Histogram equalization based methods i.e. WTHE [**93**], QDHE [**101**], RSWHE [**92**], SHMS [**104**], BHEPL [**95**] and BHEPL-D [**102**]. To analyze and compare the existing methods five test images: *Tank, U2, Field, Copter* and *Hands* are used. For performance evaluation of MMSICHE, four image quality measures are chosen, i.e. Average Luminance, Absolute Mean Brightness Error (AMBE), Average Information content (Entropy) and Back Ground Gray Level (BGL) [**114**] . Average Luminance μ is the mean gray level or brightness of the image. An algorithm is deemed to be better if average luminance of enhanced image is very close to the low-quality image. Absolute Mean Brightness Error (AMBE) is the absolute difference between the mean brightness of enhanced and the test image. The calculation of μ and *AMBE* is expressed in (5.22) and

(5.23). X_μ is the mean value of the input image, while Y_μ is the mean value of the output image.

$$\mu = \sum_{l=0}^{L-1} l \times P(l) \tag{5.22}$$

$$AMBE = \left|X_\mu - Y_\mu\right| \tag{5.23}$$

AMBE measures excessive brightness change and directly related to average luminance. For best performance, the AMBE value should be as low as possible i.e. the mean brightness of enhanced and test image should be very close. Average information content (entropy) is a measure of the richness of details of the image and usually measured in units as bits. The entropy here referred is the Shannon Entropy, and it measures of the uncertainty associated with gray levels in the image. A larger value of the entropy indicates that more information content is available in the image. Entropy $\mathrm{E(p)}$ is defined as

$$E(p) = -\sum_{i=0}^{L-1} P(i) log P(i) \tag{5.24}$$

Back Ground Gray level is the quality measure for natural enhancement. The BGL value close to the original image guarantees natural enhancement.

Table 5.1 *MMSICHE: Average luminance comparison*

Images	**Original**	**WTHE [93]**	**QDHE [101]**	**RSWHE-M [92]**	**SHMS [104]**	**BHEPL [95]**	**BHEPL-D [102]**	**MMSICHE**
Tank	132.38	212.49	162.65	124.61	131.81	154.35	33.31	134.54
U2	32.51	108.28	57.78	26.80	131.33	35.17	33.79	37.16

Field	106.39	132.81	140.17	95.22	129.02	120.29	33.25	112.76
Copter	219.46	180.22	217.31	205.43	130.52	208.73	215.62	215.96
Hands	49.13	172.07	60.58	42.44	172.47	46.78	44.07	52.21
Mean	107.97	161.17	127.69	98.90	139.03	113.06	72.00	110.52

5.1.4.1 Performance Assessment based on Image Quality Measures

Table 5.1-5.4 shows a matrix of all four IQM's for 5 test images, where rows represent the test images and the columns represent various methods used for comparison. Average luminance and AMBE are two measures, which reflect the brightness preservation capability. Table 5.1 shows Average Luminance measures for all the images using various methods. Table 5.1 reveals that the average of all images is best for MMSICHE method in terms of its closeness to the average of the original image.

Table 5.2 *MMSICHE: Average mean brightness error (AMBE) comparison*

Images	**WTHE [93]**	**QDHE [101]**	**RSWHE-M [92]**	**SHMS [104]**	**BHEPL [95]**	**BHEPL-D [102]**	**MMSICHE**
Tank	80.10	30.27	7.77	0.57	21.96	99.07	2.16
U2	75.77	25.27	5.72	98.82	2.66	1.28	4.64
Field	26.42	33.78	11.17	22.63	13.89	73.14	6.37
Copter	39.24	2.15	6.97	88.94	10.74	3.84	3.50
Hands	122.94	11.45	6.69	123.34	2.35	5.06	3.08
Mean	68.89	20.58	7.66	66.86	10.32	36.47	3.95

The average of MMSIHE is 107.97 close to the average of the original image (110.52). Specifically for Copter, Hands and Field image, the MMSICHE method produces the

images having average luminance very close to the original image. Table 5.2 shows the matrix of AMBE for all the images using various methods. Similar to average luminance MMSICHE provides best results in terms of AMBE among all methods. MMSICHE algorithm has least AMBE value for *Copter*, *Hands*, and *Field* image and further as shown in the last row the average of AMBE for all images is 3.95, which is significantly less than all other techniques. Better results in terms of Average Luminance and AMBE reflect that MMSICHE is well suited for mean brightness preservation required for consumer electronics devices.

Table 5.3 *MMSICHE: Average information content (Entropy) comparison*

Images	**Original**	**WTHE [93]**	**QDHE [101]**	**RSWHE-M [92]**	**SHMS [104]**	**BHEPL [95]**	**BHEPL-D [102]**	**MMSICHE**
Tank	5.49	4.65	5.48	4.65	5.38	5.47	2.91	5.50
U2	5.64	4.07	5.44	4.07	5.41	5.61	5.60	5.55
Field	6.56	5.28	6.53	5.28	6.50	6.53	3.86	6.56
Copter	6.31	3.75	6.24	3.75	6.11	6.21	6.19	6.22
Hands	3.99	3.20	3.91	3.20	3.60	3.96	3.97	3.98
Mean	5.60	4.19	5.52	4.19	5.40	5.55	4.51	5.56

Table 5.3 presents the entropy measures for all the techniques used in this work. MMSICHE produces highest or close to the highest entropy for all the five images thus becomes the best suitable approach for bringing out information contents of the images. Specifically for *Tank*, *Field* and *Hands* images the entropy values are almost equal to the

original image. The average of entropy produced by MMSICHE method for all images is 5.56 that are very close to average entropy (5.60) for original images; however average entropy of other methods is very less in comparison with the original image.

Table 5.4 *MMSICHE: Background gray level (BGL) comparison*

Images	**Original**	**WTHE [93]**	**QDHE [101]**	**RSWHE-M [92]**	**SHMS [104]**	**BHEPL [95]**	**BHEPL-D [102]**	**MMSICHE**
Tank	147	134	195	134	175	186	0	148
U2	22	23	20	23	101	16	16	27
Field	116	108	163	108	154	133	0	118
Copter	234	221	226	221	185	238	239	228
Hands	23	24	24	24	159	12	10	23
Mean	108	102	125	102	154	117	53	108

The entropy closer to the original image guarantees natural enhancement. Back Ground Gray Level results shown in Table 5.4 significantly outperform other techniques for all the images. The BGL values from MMSICHE method for most images are very close to the original image and ensure the natural enhancement. However, the MMSICHE method's BGL average for all the images is exactly equal to the original image.

5.1.4.2 Assessment of Visual Quality and Natural Appearance

Qualitative assessment of contrast enhancement is necessary along with quantitative assessment based on IQM's. By Visual Quality inspection, the judgment of annoying artifacts, over enhancement and unnatural enhancement can be done. Wide varieties of

standard images ranging from low-contrast to high-contrast, dark-background to bright-background are selected to show the effectiveness of the new algorithm.

The analysis of visual results from Figure 5.2-5.6 shows that the MMSICHE method produces the best results for all the images in terms of control on over enhancement as well as natural appearance. QDHE, WTHE and SHMS methods have produced over enhanced images in Figure 5.2 of Field image. However, the BHEPL-D method has introduced noise and produced annoying artifacts. The acceptable and natural enhanced images are produced by the BHEPL, RSWHE and MMSICHE. Although the MMSICHE results in Figure 5.2 for *Field* image are visually comparable to other methods but it yields the highest entropy value almost equal to the original image.

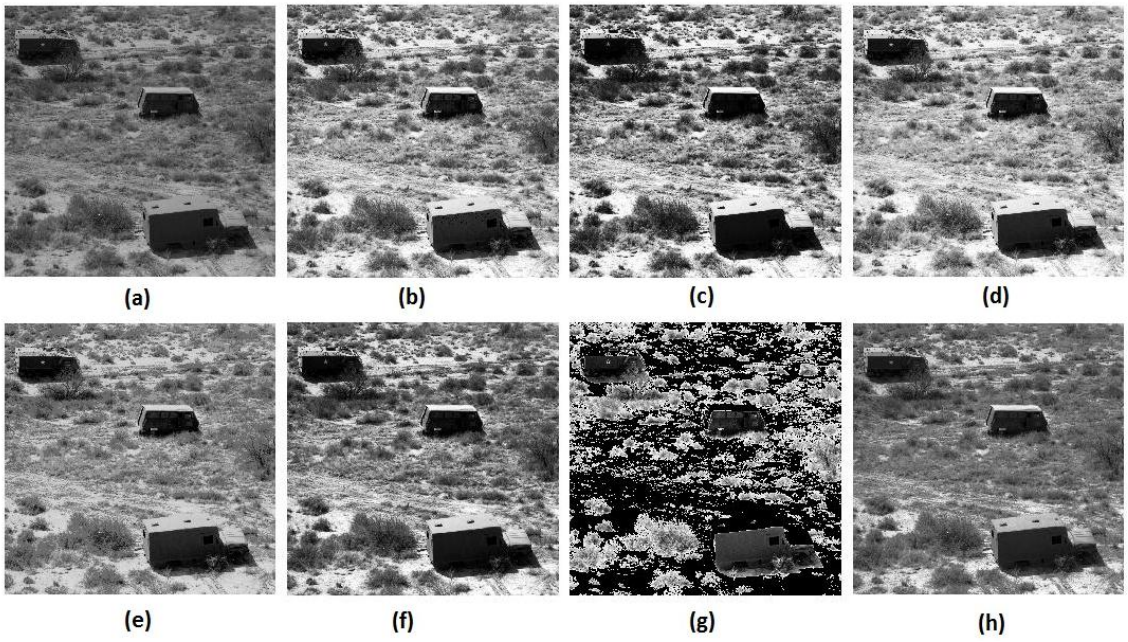

Figure 5.2 Enhancement results of different HE methods for Field image (a) Original, (b) QDHE, (c) SHMS, (d) WTHE, (e) RSWHE, (f) BHEPL, (g) BHEPL-D and (h) MMSICHE

The Copter image results in Figure 5.3 can be analyzed by viewing the copter object. The object has been darkened by WTHE and SHMS method, and overall contrast has been

reduced by these methods. MMSICHE method has produced an image with similar results of other methods.

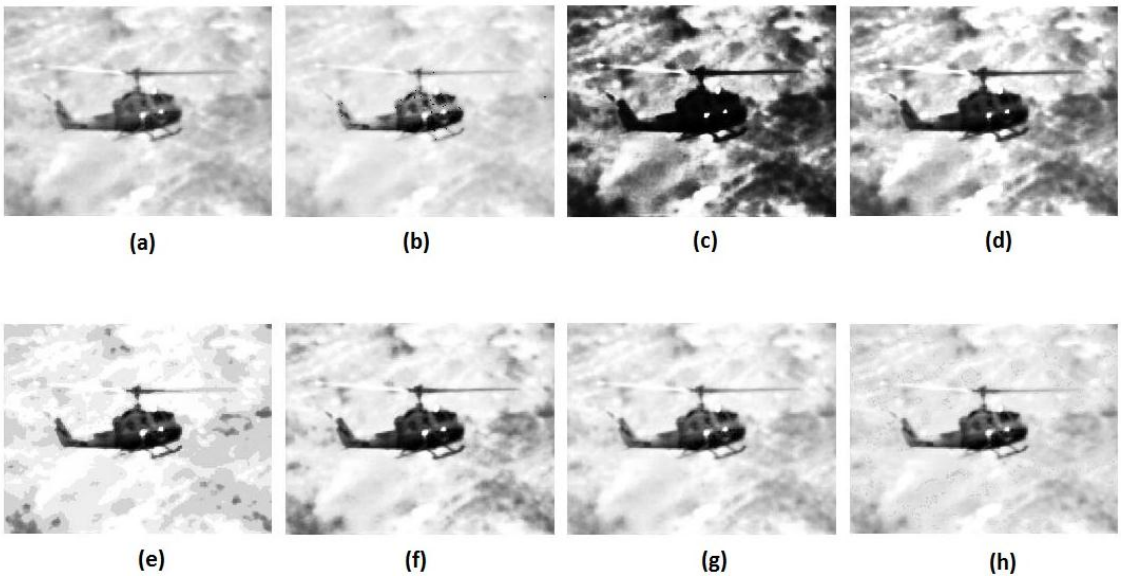

Figure 5.3 Enhancement results of different HE methods for Copter image (a) Original, (b) QDHE, (c) SHMS, (d) WTHE, (e) RSWHE, (f) BHEPL, (g) BHEPL-D and (h) MMSICHE

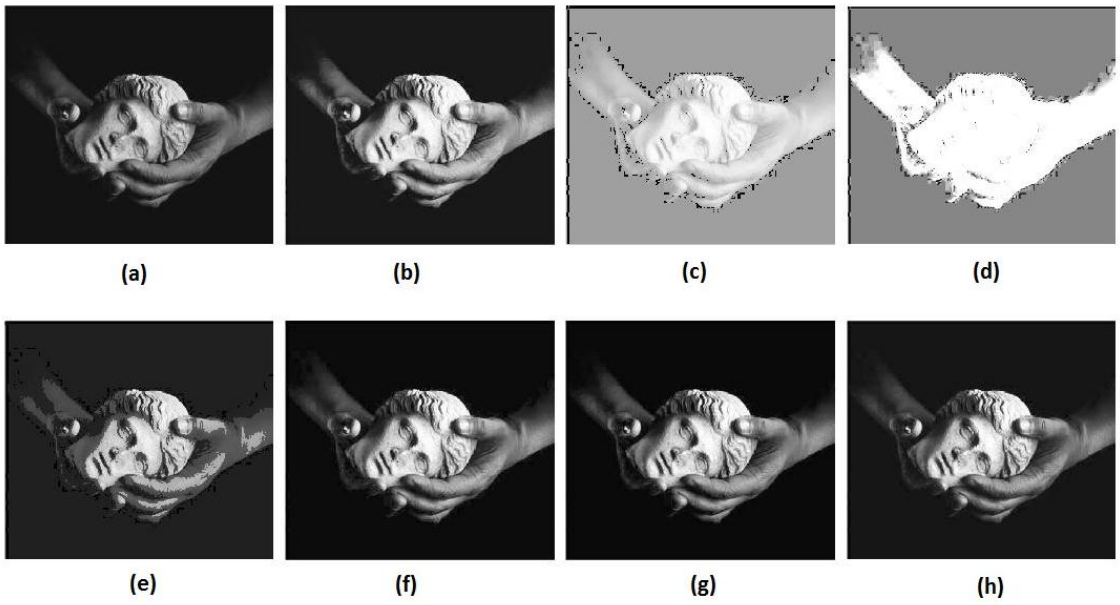

Figure 5.4 Enhancement results of different HE methods for Hands image (a) Original, (b) QDHE, (c) SHMS, (d) WTHE, (e) RSWHE, (f) BHEPL, (g) BHEPL-D and (h) MMSICHE

Similar to Copter image both WTHE and SHMS has deteriorated the Hands image in Figure 5.4 badly. RSWHE has produced over enhanced image, particularly on the finger and thumb portion. MMSICHE-ed *Hands* image is naturally enhanced image. The effectiveness of proposed method in terms of contrast enhancement can be noticed in Figure 5.5 of Tank image.

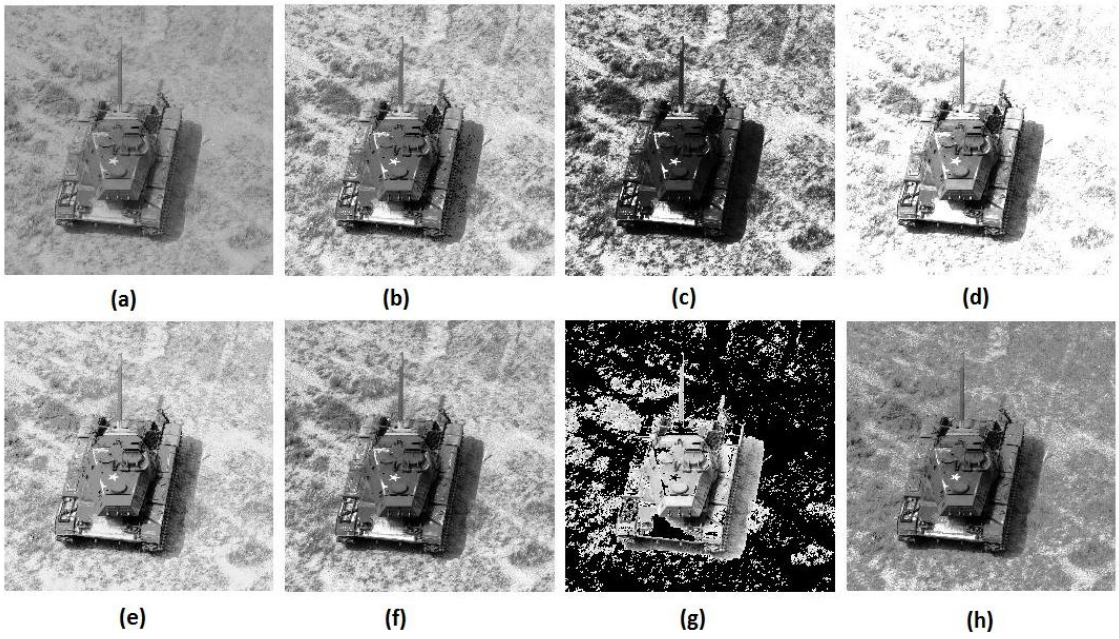

Figure 5.5 Enhancement results of different HE methods for Tank image (a) Original, (b) QDHE, (c) SHMS, (d) WTHE, (e) RSWHE, (f) BHEPL, (g) BHEPL-D and (h) MMSICHE

The original image is a low contrast image and MMSICHE yields contrast enhanced image along with natural appearance. Over-enhancement and intensity saturation phenomena have been produced by RSWHE and WTHE. SHMS output does not provide a clear vision of object in case of *Tank* image and BHEPL-D has deteriorated the image. The results in Figure 5.6 of *U2* image clearly show the superiority of MMSICHE method over other methods. It is clearly noticeable that the outputs of SHMS, WTHE, and QDHE have noise amplification. However the MMSICHE-ed image is free from noise as well as provides good contrast enhancement.

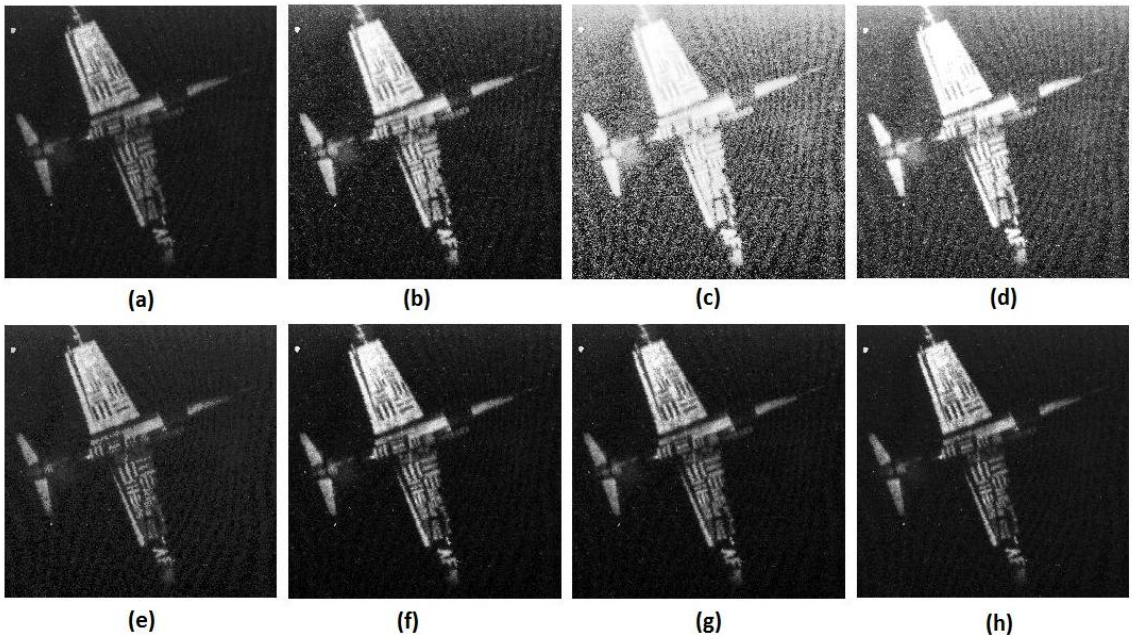

Figure 5.6 Enhancement results of different HE methods for U2 image (a) Original, (b) QDHE, (c) SHMS, (d) WTHE, (e) RSWHE, (f) BHEPL, (g) BHEPL-D and (h) MMSICHE

5.2 Exposure based Sub-image Histogram Equalization

Poor contrast images do not occupy complete dynamic range. Images having histogram bins concentrated towards lower part or the darker gray levels possess low-intensity exposure whereas images having histogram bins concentrated towards higher part or the brighter part possess high-intensity exposure. Images can be broadly classified as under exposed and over exposed based on the intensity exposure. Algorithm consists of three steps, namely Exposure thresholds calculation, Histogram Clipping and Histogram Sub division & Equalization. The description of each step is presented in the following subsections.

5.2.1 Exposure Threshold Calculation

A parameter named exposure threshold (Hanmandlu *et al*., 2009) is defined which denotes the measure of intensity exposure of the image. This parameter is being used to divide the image in under exposed and over exposed sub-images .The normalized range of exposure value is [0-1]. If the value of exposure for a particular image is more than 0.5 and tends towards 1, it means that the image has a majority of overexposed region and if this value is less than 0.5 and tending towards 0 then image is containing a majority of under exposed regions. In both cases, image contains poor contrast and need contrast enhancement. Image intensity exposure value can be calculated as Equation (5.25).

$$exposure = \frac{1}{L}\frac{\sum_{k=1}^{L} h(k)k}{\sum_{k=1}^{L} h(k)} \tag{5.25}$$

where $h(k)$ histogram of image and L is a total number of gray levels.

Another parameter X_a related to exposure is defined, which provides the value of gray level boundary that divides the image into under exposed and over exposed sub-images.

$$X_a = L(1 - exposure) \tag{5.26}$$

This parameter attains a value of greater or lesser than L/2 (gray level) for exposure value lesser or greater than 0.5 respectively for an image having dynamic range 0 to L-1.

5.2.2 Histogram Clipping

Similar to MMSICHE method, histogram clipping is also applied in ESIHE method. The clipping threshold is calculated as an average number of gray level occurrences, unlike MMSICHE where clipping threshold is calculated as the median of occupied intensity.

The formula for clipping threshold T_c is presented in (5.27) and (5.28) calculates the clipped histogram

$$T_c = \frac{1}{L}\sum_{k=1}^{L} h(k) \tag{5.27}$$

$$h_c(k) = \begin{cases} h(k), & h(k) < T_c \\ T_c, & h(k) \geq T_c \end{cases} \tag{5.28}$$

Where $h(k)$ and $h_c(k)$ are the original and clipped histogram respectively. This method of histogram clipping is computationally efficient and consumes lesser time.

5.2.3 Histogram Sub Division and Equalization

The original histogram is first bisected based on exposure threshold value X_a . The Histogram Sub Division process results in two sub-images I_L and I_U ranging from gray level 0 to X_a and $X_a + 1$ to *L-1* and can be termed as under exposed and over exposed sub-images (Figure 5.7).

$\boldsymbol{P_L(k)}$ and $\boldsymbol{P_U(k)}$ are PDF of $\boldsymbol{I_L}$ and $\boldsymbol{I_U}$ respectively

$$P_L(k) = {}^{h_c(k)}/_{N_L} \quad for\ 0 \leq k \leq\ X_a - 1 \tag{5.29}$$

$$P_U(k) = {}^{h_c(k)}/_{N_U} \qquad for\ X_a \leq k \leq\ L - 1 \tag{5.30}$$

Where $\boldsymbol{N_L}$ and $\boldsymbol{N_U}$ are a total number of pixels in sub-images $\boldsymbol{I_L}$ *and* $\boldsymbol{I_U}$ respectively. $\boldsymbol{C_L(k)}$ and $\boldsymbol{C_U(k)}$ are CDF of $\boldsymbol{I_L}$ *and* $\boldsymbol{I_U}$ respectively.

$$\boldsymbol{C_L(k)} = \sum_{\boldsymbol{k=0}}^{\boldsymbol{X_a}} \boldsymbol{P_L(k)} \tag{5.31}$$

$$C_U(k) = \sum_{k=X_a+1}^{L-1} P_U(k) \tag{5.32}$$

The next step is histogram equalization of both sub-images individually applying the transfer functions $\boldsymbol{F_L}$ *and* $\boldsymbol{F_U}$

$$F_L = X_a C_L \tag{5.33}$$

$$F_U = (X_a + 1) + (L - X_a + 1)C_U \tag{5.34}$$

The final step involves the integration of both sub-images into one complete image. The ESIHE-ed output image is produced by the combination of both transfer functions for further visual quality inspection and performance evaluation.

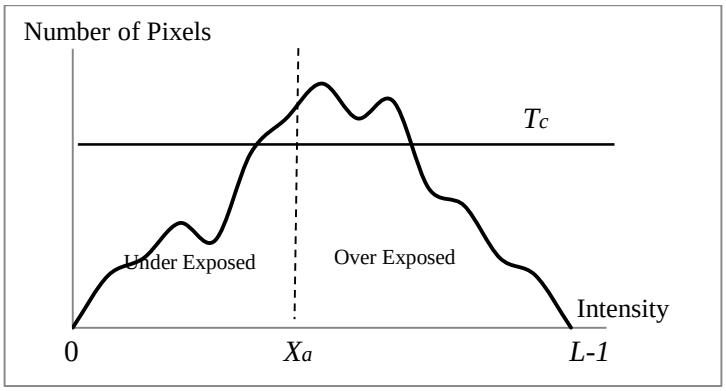

Figure 5.7 ESIHE: Process of Histogram Sub Division and Clipping

Algorithm 5.1: ESIHE Algorithm
Step 1: Compute the histogram *h(k)* of the image. **Step 2:** Compute the value of exposure and threshold parameter X_a. **Step 3:** Compute the clipping threshold T_c and clip the histogram $h_c(k)$. **Step 4:** Divide the clipped histogram into two sub-histograms using the threshold parameter X_a.

Step 5: Apply the histogram equalization on individual sub-histograms.

Step 6: Combine the sub-images into one image for analysis.

5.2.4 Simulation Results of ESIHE Method

The simulation results of proposed ESIHE method are compared with existing histogram equalization methods i.e. BBHE [**87**], MMBEBHE [**89**], DSIHE [**88**], RMSHE [**90**] and RSIHE [**91**]. To analyze and compare the existing methods nine test images: Hands, Fish, Mosque, Tank, Cat, Butterfly, Aircraft, Couple, and Field are used. Visual quality comparison of four images i.e. Hands, Fish, Tank, and Cat is shown in Figure 5.8-5.11. To evaluate the performance of ESIHE, Average Information content is being used as image quality measure. An image with higher entropy value had richness in details and perceived to have better quality.

5.2.4.1 Performance Assessment based on Average Information Content

The discrete entropy computed for the methods used in this work for all 9 images are tabulated in Table 5.5. ESIHE produces the highest entropy for all the images thus becomes best suitable approach for bringing out information contents of the image. Specifically for Butterfly, aircraft, Mosque and fish image the entropy values are almost equal to the original image. However for HE and MMBEBHE the entropy value for all the images is very less then the corresponding original image. DSIHE method that claimed superior performance in terms of the average information content of the image is having entropy values lesser than the proposed method. The average of entropy produced by ESIHE method for all images is 5.39 that is very close to average entropy (5.43) for original images. However, average entropy of other methods is much smaller in

comparison with the original image. The entropy closer to original image guarantees bringing out maximum information content of the image.

5.2.4.2 Assessment of Visual Quality

Qualitative assessment of contrast enhancement is necessary along with quantitative assessment. The enhancement results can only be appreciated if the resultant image gives pleasing effect in appearance. By visual quality inspection, the judgment of annoying artifacts, over enhancement and unnatural enhancement can be done.The visual assessment results are effective quality measures to judge the performance of contrast enhancement algorithm.

Table 5.5 *ESIHE: Entropy Comparison of Different Methods*

Images	**Original**	**HE**	**BBHE [87]**	**MMBEBHE [89]**	**DSIHE [88]**	**RSIHE [91]**	**RMSHE [90]**	**ESIHE**
Butterfly	4.89	4.70	4.83	4.78	4.83	4.81	4.86	4.89
Aircraft	4.00	3.75	3.90	3.86	3.87	3.95	3.94	3.99
Tank	5.49	4.97	5.42	5.31	5.38	5.45	5.46	5.47
Field	6.56	5.96	6.46	6.41	6.46	6.52	6.49	6.52
Fish	4.49	4.43	4.38	4.22	4.48	4.43	4.48	4.49
Cat	6.01	4.85	5.62	5.64	5.69	5.85	5.68	5.88
Hands	3.99	2.89	3.73	3.79	3.86	3.55	3.80	3.92
Mosque	6.26	5.83	6.11	6.06	6.09	6.08	6.10	6.26
Couple	7.20	5.96	7.01	7.01	7.01	7.06	7.04	7.12
Mean	5.43	4.82	5.27	5.23	5.30	5.30	5.32	5.39

Wide varieties of a test set of images including under-exposed, over-exposed, low-contrast, high-contrast, dark-background, and bright-background are chosen to judge the robustness and versatility of ESIHE method. The analysis of visual results from Figure 5.8-5.11 shows the supremacy of ESIHE for all test images not only in terms of contrast enhancement but also in terms of control on over-enhancement. The effectiveness of proposed method in terms of contrast enhancement can be noticed in Figure 5.8 of *Hands* image.

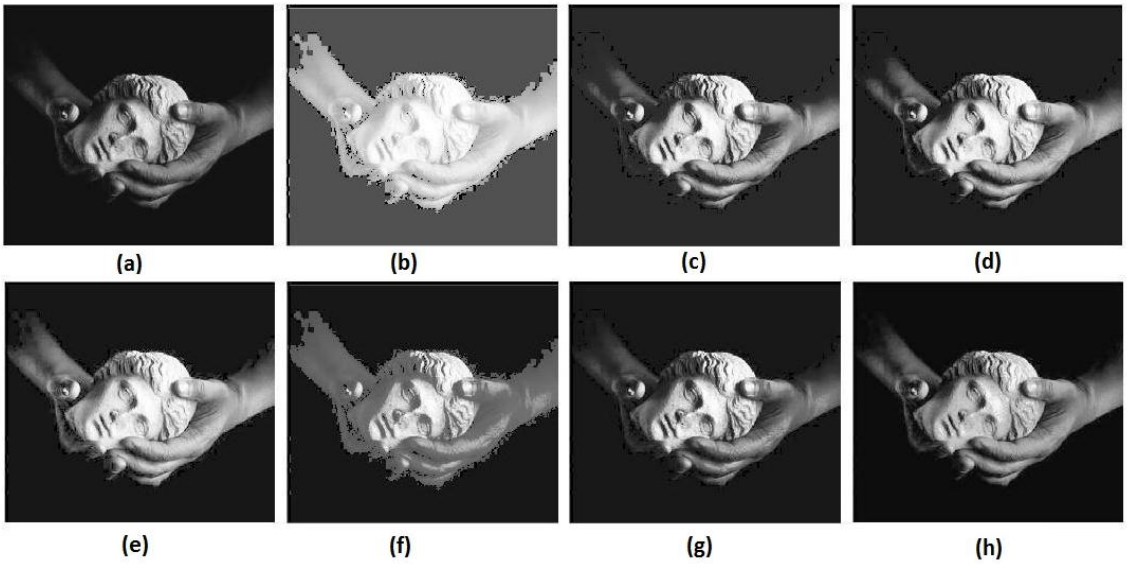

Figure 5.8 Enhancement results of different HE methods for Hands image (a) Original, (b) HE, (c) BBHE, (d) MMBEBHE, (e) DSIHE, (f) RSIHE, (g) RMSHE and (h) ESIHE

HE, DSIHE and RSIHE results of *Hands* image are over enhanced. However, ESIHE image controls over-enhancement that leads to natural enhancement results.The original *Fish* image in Figure 5.9 is low exposed image even though ESIHE has improved the quality of image in a big way. The objects in ESIHE-ed *Fish* image are clearly visible

however except HE, other methods are not able to enhance the image and object, as well as background, is not clearly visible in enhanced images.

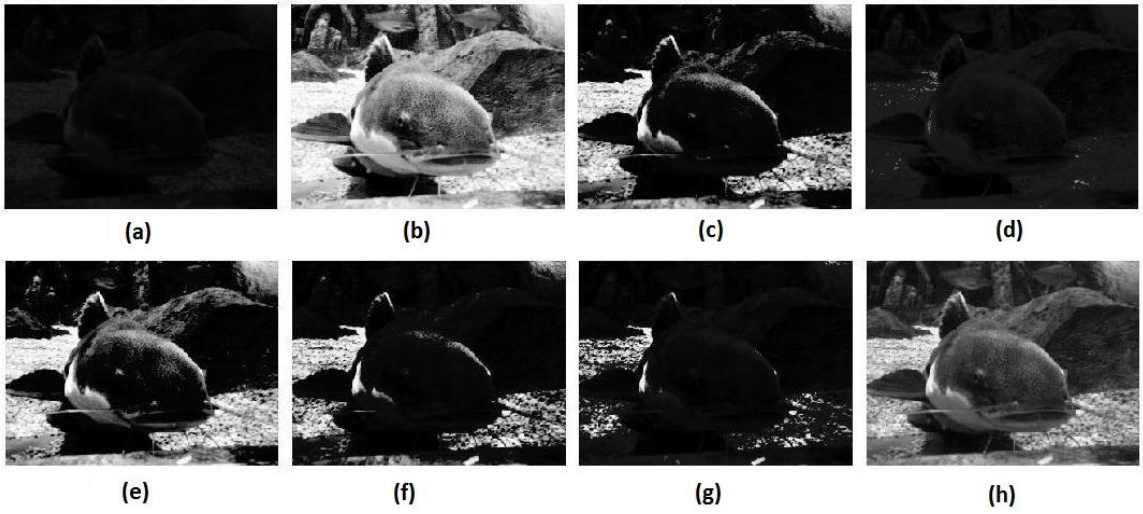

Figure 5.9 Enhancement results of different HE methods for Fish image: (a) Original, (b) HE, (c) BBHE, (d) MMBEBHE, (e) DSIHE, (f) RSIHE, (g) RMSHE and (h)ESIHE

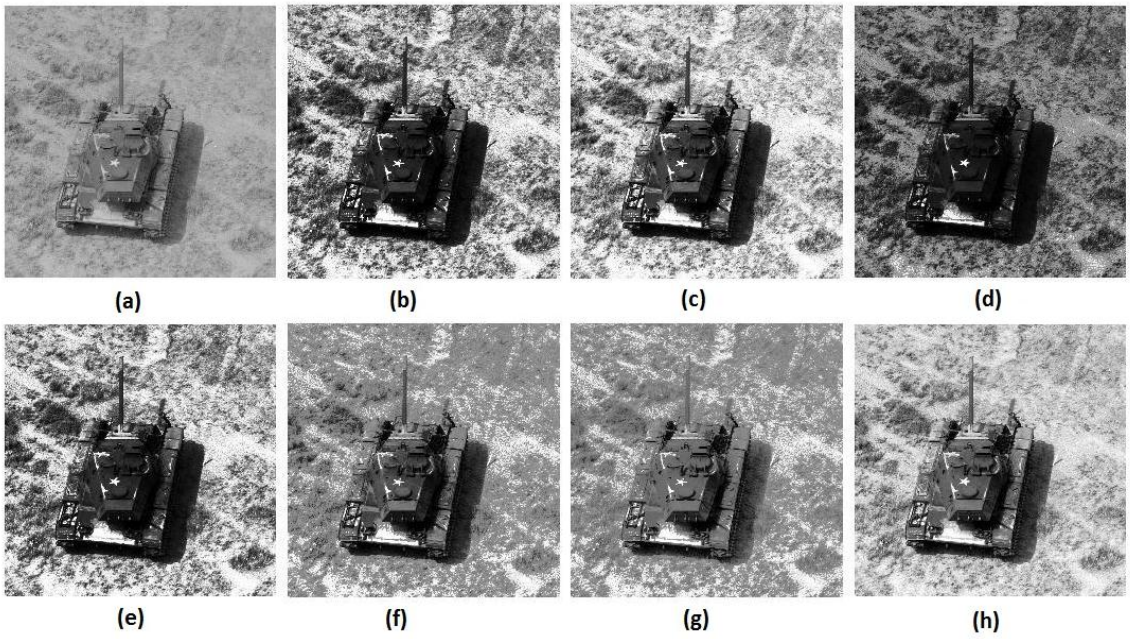

Figure 5.10 Enhancement results of different HE methods for Tank image: (a) Original, (b) HE, (c) BBHE, (d) MMBEBHE, (e) DSIHE, (f) RSIHE, (g) RMSHE and (h)ESIHE

The *Tank* image in Figure 5.10 is a low contrast image and ESIHE yields contrast enhanced image along with natural appearance. The HE, BBHE, DSIHE and MMBEBHE outputs don't provide clear vision of object in case of *Tank* image. From Figure 5.11 of *Cat* image it is clearly noticeable that the ESIHE-ed image enhances the low exposed part of image i.e. the left ear of the cat effectively.

Although the ESIHE results in Figure 5.11 for *Cat* image and Figure 5.10 for *Tank* image are visually comparable to other methods but proposed method yields highest entropy value for these images. This shows that ESIHE method produces images with the richness of details.

Figure 5.11 Enhancement results of different HE methods for Cat image: (a) Original, (b) HE, (c) BBHE, (d) MMBEBHE, (e) DSIHE, (f) RSIHE, (g) RMSHE and (h)ESIHE

5.3 Recursive Histogram Equalization for Low Exposure Images

In the past various techniques are proposed to cater the problems of brightness preservation and over enhancement, but low exposure image enhancement is still a gray area. Two extensions of the ESIHE are proposed. First, a recursive method is proposed as the extension of the ESIHE, called Recursive Exposure based sub-image histogram

equalization (R-ESIHE). The proposed method iteratively performs ESIHE on the image until the difference of exposure values between subsequent iterations is less than a threshold value. The second method is Recursively separated Exposure based sub-image histogram equalization (RS-ESIHE). Unlike the R-ESIHE, the second algorithm first splits the histogram into two or more sub-histograms based on the individual exposure thresholds and then performs histogram equalization of all the sub-histograms. Clipping of histogram is added in both the proposed methods to avoid excessive enhancement. Both algorithms are described in the following sections.

5.3.1 Recursive Exposure based Sub-Image Histogram Equalization

The proposed RESIHE method is a recursive variant of ESIHE, which performs ESIHE recursively on the given histogram. The number of recursions is dependent on the exposure difference between successive iteration. The number of iterations is decided based on a threshold £ whose value is normally taken very less (here 0.01).

Algorithm 5.2: RESIHE Algorithm
Step 1: Calculate the histogram $h(k)$. **Step 2:** Calculate the exposure threshold parameter X_a. **Step 3:** Calculate the clipping threshold T_c and clip the histogram $h_c(k)$. **Step 4:** Partition the histogram into two sub-histograms using the threshold parameter X_a. **Step 5:** Equalize each sub-histogram individually.

Step 6: Integrate the sub-images to yield enhanced image.

Step 7: Repeat step 1-6 until the exposure difference between successive iterations is less than threshold £.

5.3.2 Recursively Separated Exposure based Sub-Image Histogram Equalization

Conceptually, RS-ESIHE performs recursive decomposition of the histogram. ESIHE decomposes the input histogram only once based on the exposure threshold while RS-ESIHE decomposes it recursively based on exposure thresholds of individual sub-histograms up to a recursion level r, generating $\mathbf{2^r}$ sub-histograms. The decomposed sub-histograms are then equalized individually. For simplicity recursion level, r is taken as two. The RS-ESIHE method comprises of Exposure Threshold calculations, Histogram Clipping, and Sub-histogram computation & Equalization.

5.3.2.1 Exposure Threshold Calculations

The exposure threshold $\boldsymbol{X_a}$of complete histogram is calculated as per ESIHE method. Two more exposure thresholds ($\boldsymbol{X_{al}}$ and $\boldsymbol{X_{au}}$) are calculated for two individual sub-histogram divided based on $\boldsymbol{X_a}$.

$$X_{al} = L\left[\frac{X_a}{L} - \frac{\sum_0^{Xa-1} h(k)k}{L\sum_0^{Xa-1} h(k)}\right] \tag{5.35}$$

$$X_{au} = L\left[1 + \frac{X_a}{L} - \frac{\sum_{Xa}^{L-1} h(k)k}{L\sum_{Xa}^{L-1} h(k)}\right] \tag{5.36}$$

5.3.2.2 Sub-histogram Computation and Equalization

The histogram is first partitioned into two sub-images based on exposure threshold value X_a. These individual sub-histograms are further decomposed into two smaller sub-histograms where the individual exposure threshold X_{al} and X_{au} acts as the separating point of sub-histograms. The sub-histogram computation process results in four sub-imagesW_{Ll}, W_{Lu} , W_{Ul} and W_{Uu} ranging from gray level 0 to $X_{al}-1$, X_{al} to X_a-1, X_a to $X_{au}-1$, X_{au} to L-1. $P_{Ll}(k)$,$P_{Lu}(k)$,$P_{Ul}(k)$ and $P_{Uu}(k)$ are PDF of W_{Ll}, W_{Lu} , W_{Ul} and W_{Uu} respectively.

$$P_{Ll}(k) = {h_c(k)}/{N_{Ll}} \; for \; 0 \le k \le X_{al}-1 \tag{5.37}$$

$$P_{Lu}(k) = {h_c(k)}/{N_{Lu}} \; for \; X_{al} \le k \le X_a-1 \tag{5.38}$$

$$P_{Ul}(k) = {h_c(k)}/{N_{Ul}} \; for \; X_a \le k \le X_{au}-1 \tag{5.39}$$

$$P_{Uu}(k) = {h_c(k)}/{N_{Uu}} \; for \; X_{au} \le k \le L-1 \tag{5.40}$$

$\boldsymbol{N_{Ll}, N_{Lu}, N_{Ul}}$ and $\boldsymbol{N_{Uu}}$ are the total number of pixels in sub-images $\boldsymbol{W_{Ll}}$, $\boldsymbol{W_{Lu}}$, $\boldsymbol{W_{Ul}}$ and $\boldsymbol{W_{Uu}}$ respectively. $\boldsymbol{C_{Ll}(k)}$,$\boldsymbol{C_{Lu}(k)}$,$\boldsymbol{C_{Ul}(k)}$ and $\boldsymbol{C_{Uu}(k)}$ are CDF of $\boldsymbol{W_{Ll}}$, $\boldsymbol{W_{Lu}}$, $\boldsymbol{W_{Ul}}$ *and* $\boldsymbol{W_{Uu}}$and respectively as defined in (5.41-5.44)

$$C_{Ll} = \sum_{k=0}^{X_{al}-1} P_{Ll}(k) \tag{5.41}$$

$$C_{Lu} = \sum_{k=X_{al}}^{X_a-1} P_{Lu}(k) \tag{5.42}$$

$$C_{Ul} = \sum_{k=X_a}^{X_{au}-1} P_{Ul}(k) \tag{5.43}$$

$$C_{Uu} = \sum_{k=X_{au}}^{L-1} P_{Uu}(k) \tag{5.44}$$

The next step of RS-ESIHE is to perform histogram equalization of all the four sub-histograms individually. The transfer functions F_{Ll}, F_{Lu}, F_{Ul} *and* $F_{Uu}$for sub-histogram equalization are defined as below

$$F_{Ll} = X_{al} C_{Ll} \tag{5.45}$$

$$F_{Lu} = (X_{al} + 1) + (X_a - X_{al} + 1) C_{Lu} \tag{5.46}$$

$$F_{Ul} = (X_a + 1) + (X_{au} - X_a + 1) C_{Ul} \tag{5.47}$$

$$F_{Uu} = (X_{au} + 1) + (L - X_{au} + 1) C_{Uu} \tag{5.48}$$

The final step of RS-ESIHE to perform integration of all four transfer functions to yield resultant image.

Algorithm 5.3: RS-ESIHE Algorithm
Step 1: Calculate the histogram $h(k)$. **Step 2:** Calculate the exposure threshold parameter X_a. **Step 3:** Calculate the clipping threshold T_c and clip the histogram $h_c(k)$. **Step 4:** Partition the histogram into two sub-histograms using the threshold parameter X_a **Step 5:** Calculate exposure thresholds X_{al} and X_{au} for lower and upper sub-histograms respectively and divide the sub-histograms into further sub-histograms using X_{al} and X_{au} as decomposing threshold, resulting in total four sub-histograms.

Step 6: Equalize individual sub-histograms and integrate all the sub-images to yield enhanced image.

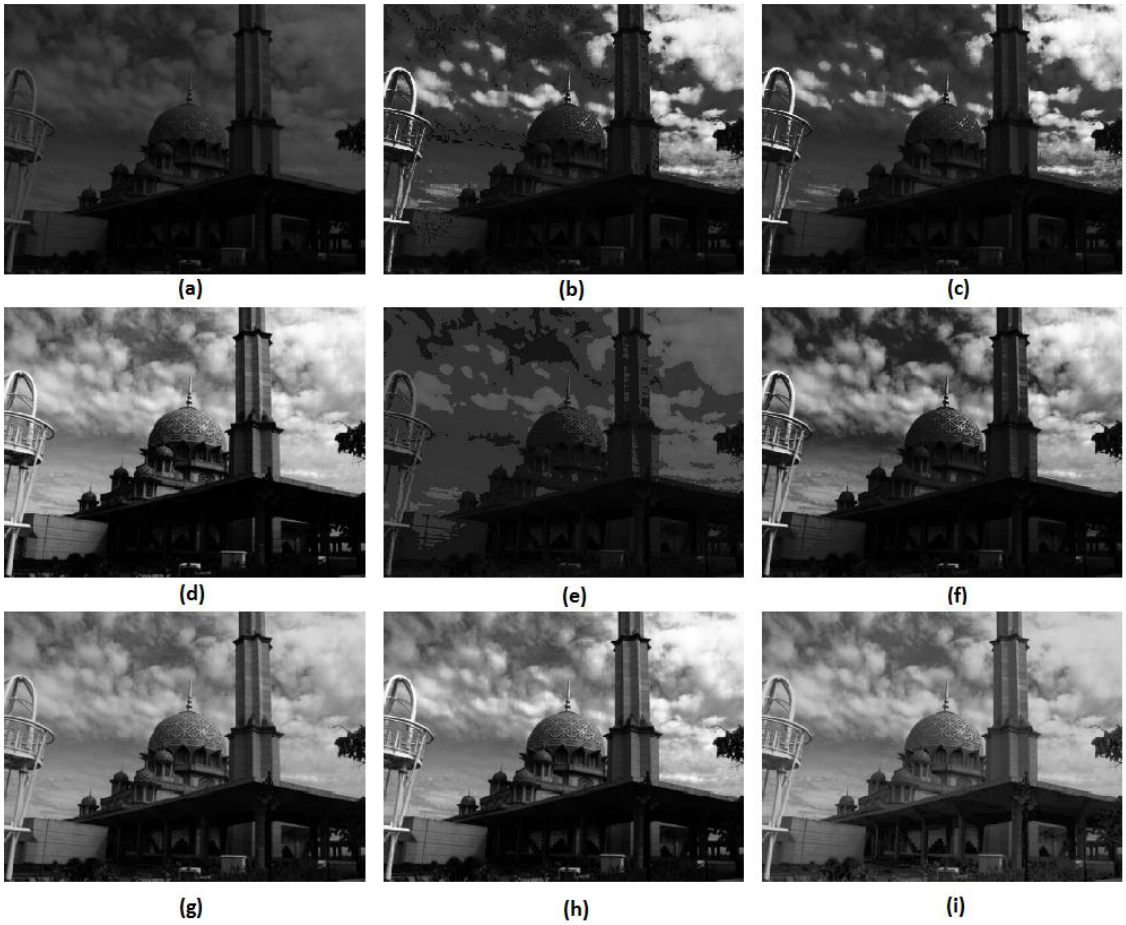

Figure 5.12 Visual quality comparison of different HE methods for Mosque image (a) Original, (b) RSIHE, (c) RMSHE, (d) QDHE, (e) RSWHE, (f) BHEP-L, (g) ESIHE, (h) RESIHE and (i) RS-ESIHE

5.3.3 Simulation Results of RESIHE and RS-ESIHE

The performance of proposed methods is compared with other HE based methods i.e. RMSHE **[**90**]**, RSIHE **[**91**]**, QDHE **[**101**]**, RSWHE **[**92**]**, BHEPL **[**95**]** and ESIHE **[**112**]**. In order to appreciate the results, four low exposure test images: *Fish1*, *Fish2 Mosque* and

Couple are taken for analysis. Both fish images are underwater sequence while other two images are captured in low light conditions.

5.3.3.1 Visual Quality Performance Comparison

Images acquired in low light conditions including under water sequences are taken to test the robustness of the proposed method for low exposure imaging. From the inspection of visual results in Figure 5.12-5.15, it is evident that the proposed recursive methods are very effective especially in low light conditions.

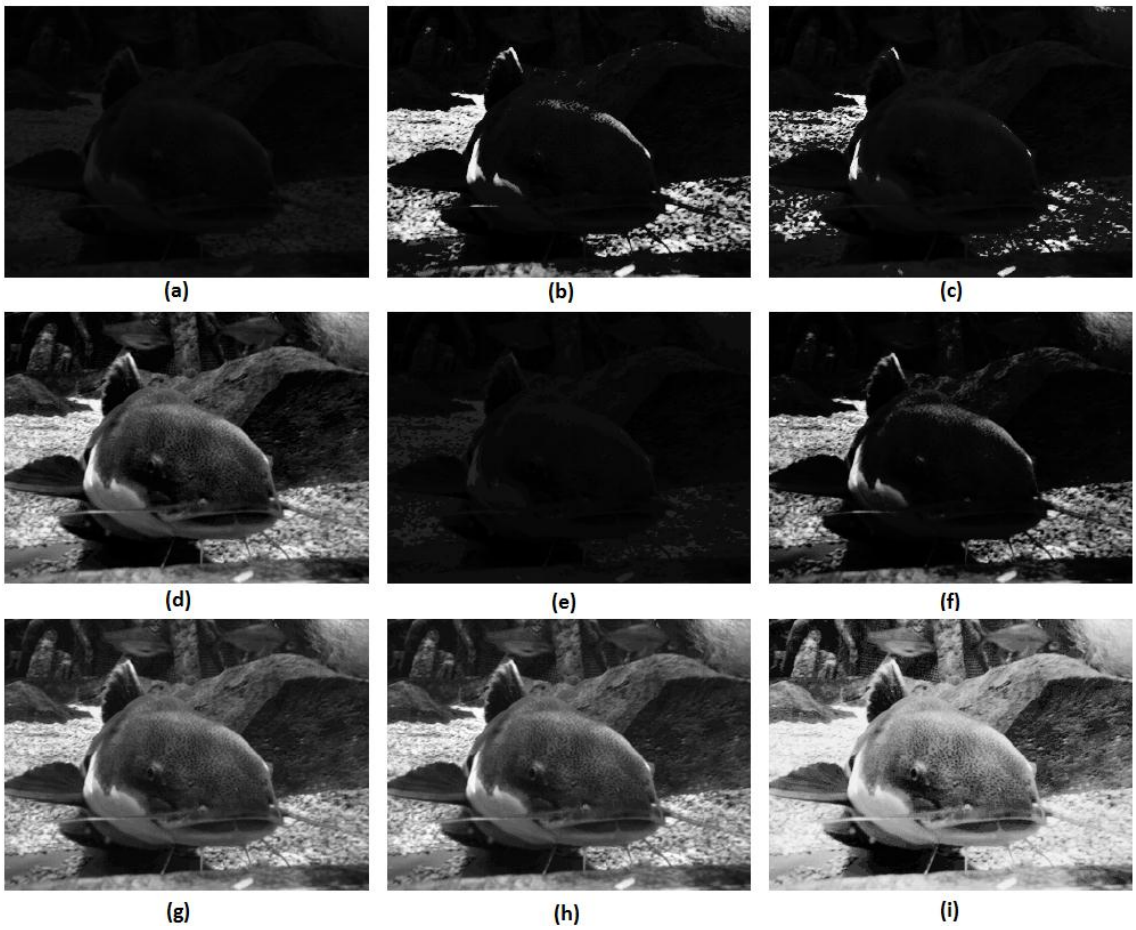

Figure 5.13 Visual quality comparison of different HE methods for Fish2 image (a) Original, (b) RSIHE, (c) RMSHE, (d) QDHE, (e) RSWHE, (f) BHEP-L, (g) ESIHE , (h) RESIHE and (i) RS-ESIHE

Contrast enhancement results can be clearly appreciated by observing the visual quality results in Figure 5.12 of Mosque image. RSIHE, RMSHE, RSWHE and BHEP-L methods are not able to increase the exposure. However, both RESIHE and RS-ESIHE has improved the contrast and the objects are clearly visible. In both the underwater images i.e. Fish1 and Fish2 in Figure 5.13 and Figure 5.15 respectively the original images are acquired in very dim light condition and the object is not clearly visible.

Figure 5.14 Visual quality comparison of different HE methods for Couple image (a) Original, (b) RSIHE, (c) RMSHE, (d) QDHE, (e) RSWHE, (f) BHEP-L, (g) ESIHE , (h) RESIHE and (i) RS-ESIHE

The resultant Fish images of proposed methods have the objects clearly distinguishable. The proposed algorithms enhance the overall image quality of couple image as shown in Figure 5.15. Low-intensity regions in the background are properly exposed resulting clear vision.

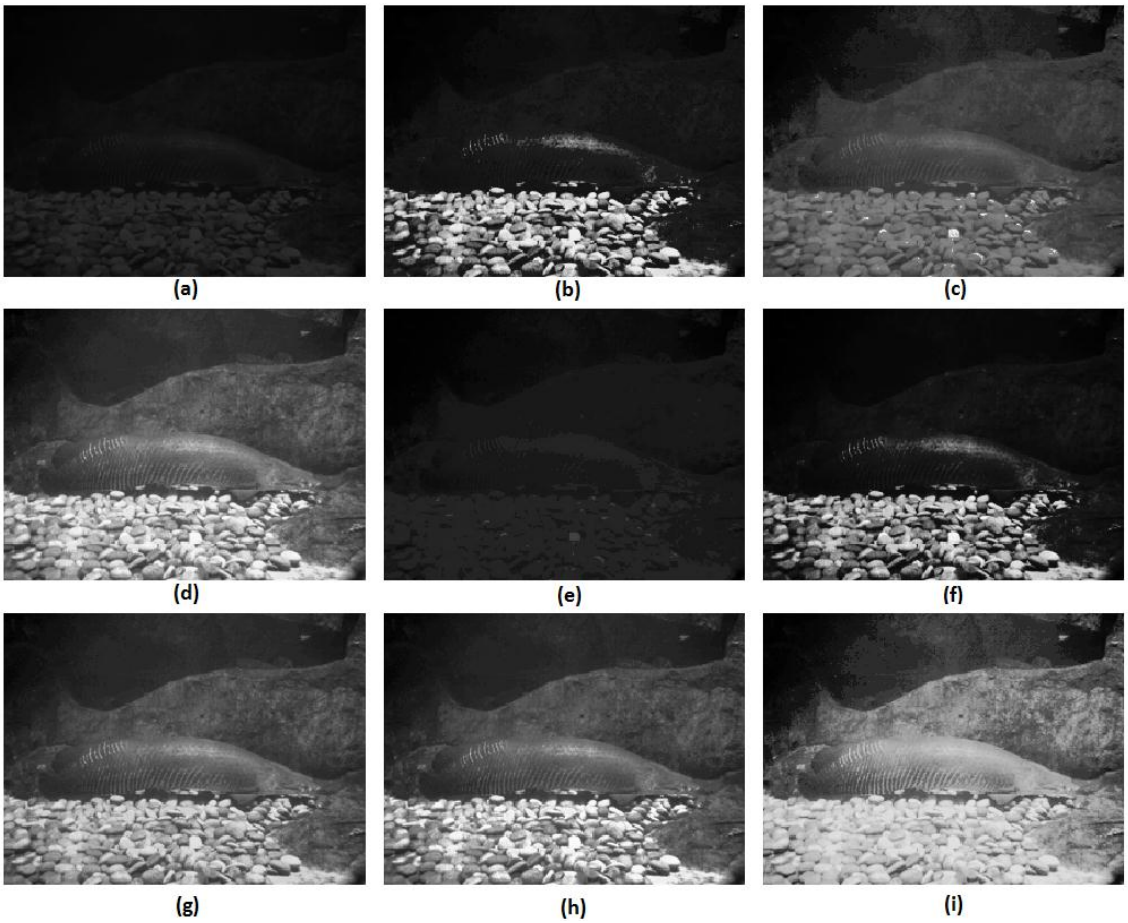

Figure 5.15 Visual quality comparison of different HE methods for Fish1 image (a) Original, (b) RSIHE, (c) RMSHE, (d) QDHE, (e) RSWHE, (f) BHEP-L, (g) ESIHE , (h) RESIHE and (i) RS-ESIHE

5.3.3.2 Performance Comparison based on Entropy

For assessment of the performance of the proposed algorithms, we have chosen entropy as the quality measure. Entropy measures the richness of information in an image. When an enhanced image has higher entropy value, then the details of the input image are said to be preserved in the output image.

The entropy results of various methods for all the four images taken for experimentation tabulated in Table 5.6. For optimum performance, the entropy should be as close as possible to the original image. The proposed new methods produce images with entropy very close to the original one thus becomes well suited for preserving details of the input image.

Table 5.6 *RESIHE, RS-ESIHE: Entropy Comparison of Different Methods*

Images	**Original**	**QDHE [101]**	**BHEP-L [95]**	**RSWHE [92]**	**ESIHE [112]**	**RESIHE**	**RS-ESIHE**
Fish1	5.050	5.043	5.042	3.323	5.046	5.048	5.047
Fish2	4.490	4.477	4.479	3.127	4.480	4.487	4.483
Couple	6.398	6.279	6.321	4.559	6.299	6.338	6.284
Mosque	6.263	6.101	6.217	4.599	6.220	6.259	6.232
Mean	5.550	5.479	5.517	3.902	5.521	5.533	5.524

5.4 Significant Findings

The proposed four HE based histogram equalization methods achieved the research objectives and the main contribution in this chapter can be summarized as below:

(a) In ESIHE method, exposure based division of image and histogram equalization of sub-images proved very effective technique for enhancing under exposed images. The histogram clipping technique combined with histogram equalization provided control on over enhancement leading to natural enhancement.

(b) The visual quality of resultant images of exposure based recursive HE methods (R-ESIHE & RS-ESIHE) shows the robustness of the method on low light images.

(c) MMSICHE technique which achieves the multiple objectives of entropy maximization, brightness preservation, and control over enhancement, is a better approach to natural image enhancement.

This chapter is based on the following work:

1) ***Kuldeep Singh**, Rajiv Kapoor, "Image enhancement using Exposure based Sub Image Histogram Equalization", Pattern Recognition Letters(Elsevier , Impact factor-1.896) 36 (2014) 10 – 14 (DOI:10.1016/j.patrec.2013.08.024)* [**112**]

2) ***Kuldeep Singh**, Rajiv Kapoor, "Image enhancement via Median-Mean Based Sub-Image-Clipped Histogram Equalization", Optik- Int. J. Light Electron Opt., (Elsevier Impact factor-0.670) 125 (2014) 4646-4651 (DOI: 10.1016/j.ijleo.2014.04.093)* [**111**]

3) ***Kuldeep Singh,** Rajiv Kapoor, Sanjeev Kr. Sinha,"Enhancement of low Exposure Images via Recursive Histogram Equalization Algorithms", Optik- Int. J. Light Electron Opt., (Elsevier, Impact factor-0.670) 126 (2015) 2619–2625 (DOI:10.1016/j.ijleo.2015.06.060)* [**113**]

CHAPTER 6

CONCLUSION AND FUTURE SCOPE OF WORK

Image enhancement algorithms that include image denoising, superresolution, and contrast enhancement are indispensable to the field of image processing and computer vision. In this dissertation, these image quality improvement techniques have been discussed. In this chapter, the major contributions, achievements, and future scope of work of the thesis are summarized.

6.1 Summary

This thesis has investigated fingerprint image quality improvement through sparse representation based denoising and superresolution algorithms. The problem of low exposure imaging is addressed through histogram equalization. There were three main threads to this research: sparse representation based fingerprint denoising, sparse representation based fingerprint superresolution and contrast enhancement. Novel contributions made in this research are summarized as follow:

- A novel algorithm is proposed for constructing ridge orientation based sparse sub-dictionary that exploits the self-similarity among fingerprint patches. Instead of having a single dictionary, the proposed method clusters the training patches into groups based on ridge orientation of patch. Since every sub-group consists of geometrically similar patches, thus, the sub-dictionary trained from them can

work more effectively, and this will help in improving denoising and superresolution performance. Use of sub-dictionaries based on dominant orientation significantly improves the effectiveness of sparse modeling of information in a fingerprint image in the form local ridge patterns.

- A novel denoising algorithm specific to fingerprint image is proposed using ridge orientation based clustered sub-dictionaries. Adaptive selection of suitable sub-dictionary while reconstruction based on minimum residue error criterion is embedded in the algorithm to enhance the performance of denoising algorithm. Experimental results demonstrate that the proposed approach can be very helpful in denoising of fingerprints and can provide aid to automatic fingerprint identification systems.
- In this thesis, the area of fingerprint superresolution is explored. A novel sparse superresolution algorithm using ridge orientation based clustered coupled sub-dictionaries is developed. Instead of having a single dictionary, the proposed method clusters the training patches into six groups based on ridge orientation of patch, including one group for flat patches to train six coupled sub-dictionaries. By jointly training coupled sub-dictionaries for the low and high-resolution image patches, the similarity of sparse representations between the low-resolution and high-resolution image patch pair with respect to their own dictionaries can be enforced. Atoms from sub-dictionary with minimum residue error are used during reconstruction of patches. The iterative back projection method is also incorporated in the final step of the algorithm to eliminate discrepancy due to noise or inaccuracy in sparse representation. Experimental

results also prove that this approach of superresolution is far superior for fingerprint images than traditional superresolution methods in terms of fingerprint matching and is more robust when the scaling factor is large.

- The problem of low exposure imaging is addressed using exposure based sub-histogram equalization techniques. A novel method for sub division of image histogram into under-exposed and over-exposed based on the exposure related parameter is proposed. Exposure-based division of image and histogram equalization of sub-images proved very effective technique for enhancing under-exposed images. The deciding factor for the division of image depends on exposure value, and it possess values greater then L/2 grey level for under exposed images (exposure value less than 0.5) and compensates for low exposure by introducing higher grey levels in sub-image so that after individual histogram equalization process the overall exposure value increases. The inverse is true for the over exposed images where the sub division of images is done on the grey level lesser than L/2 grey level. Over enhancement is controlled by histogram clipping approach by restricting the enhancement rate. The entropy measures of the proposed ESIHE method clearly show that it outperforms other HE based methods. The Visual quality of ESIHE-ed images shows the robustness of the method and supremacy on other methods for a wide variety of low exposure images.

- Two recursive variants of exposure based sub-histogram equalization techniques are proposed here for enhancement of low exposure images. These methods can be very effective for contrast enhancement of images acquired in dim light

conditions i.e. under water or night vision images. Better results in terms of entropy make these methods more suitable in terms of richness in details. The visual quality of resultant images of recursive methods shows the robustness of the method on low light images.

- Another variant of histogram equalization i.e. MMSICHE has been proposed for the preservation of brightness and entropy along with control over enhancement simultaneously. The bisection of histogram first based on median then based on mean plays the role of preservation of mean brightness and entropy simultaneously. In this method clipping of histogram provides control on over enhancement. Simulation results clearly show that MMSICHE outperforms other HE based methods in terms of image quality measures. Visual quality assessment results also prove the supremacy of MMSICHE over other methods in terms of natural enhancement.

6.2 Future Scope of Work

This thesis addressed several questions of image quality improvement. However, there are also other questions, which are being currently investigated and which have not been presented in this thesis. This research work gives rise to several possible improvements and future research directions.

Sparse representation based fingerprint image quality improvement has shown promising results. However, the sparse coding is a time-consuming algorithm and need special attention of researchers. For practical implementation of sparse coding-based fingerprint quality improvement, there is a need of improvement in time complexity of

these algorithms. Nevertheless, the effectiveness and efficiency of sparse representation methods cannot perfectly meet the need for real-world applications. Enhancing the robustness of sparse representation can be considered as another indispensable problem when researchers design algorithms.

Another interesting research problem is how to extend the current sparse representation based formulation for solving blind image deblurring problems. Applying geometrically clustered sub-dictionaries for other applications such as inpainting, demosaicing, denoising of video, and more, are all interesting directions that could and should be explored.

In histogram equalization based contrast enhancement methods, the enhanced image often contains undesirable artifacts because an excessive number of pixels in the non-textured areas heavily bias the histogram. In the process of histogram equalization, the impact of the pixels in non-textured areas should be suppressed, and the texture features can be exploited for the computation of histogram.

BIBLIOGRAPHY

[1] Leonid I. Rudin, Stanley Osher, and Emad Fatemi, "Nonlinear total variation based noise removal algorithms," *Physica D: Nonlinear Phenomena*, vol. 60, no. 1-4, pp. 259-268, November 1992.

[2] D. Geman and G. Reynolds, "Constrained restoration and the recovery of discontinuities," *IEEE Trans. Pattern Anal. Mach. Intell.*, vol. 14, no. 3, pp. 367–383, March 1992.

[3] D. Mumford and J. Shah, "Optimal approximations by piecewise smooth functions and associated variational problems," *Commun. Pure Appl. Math.*, vol. 42, no. 5, pp. 577–685, Jul. 1989.

[4] Jian Zhang, Debin Zhao, and Wen Gao, "Group-Based Sparse Representation for Image Restoration," *IEEE Trans. Image Process.*, vol. 23, no. 8, pp. 3336-3351, Aug. 2014.

[5] Michael Elad and Michal Aharon, "Image Denoising Via Sparse and Redundant Representations Over Learned Dictionaries," *IEEE Trans. Image Process.*, vol. 15, no. 12, pp. 3736-3745, Dec. 2006.

[6] Weisheng Dong, Lei Zhang, Guangming Shi , and Xiaolin Wu, "Image Deblurring and Super-Resolution by Adaptive Sparse Domain Selection and Adaptive Regularization," *IEEE Trans. Image Process.*, vol. 20, no. 7, pp. 1838-1857, Jul. 2011.

[7] Jianchao Yang , John Wright, Thomas Huang, and Yi Ma, "Image Super-Resolution Via Sparse Representation," *IEEE Trans. Image Process.*, vol. 19, no. 11, pp. 2861-2873, Nov. 2010.

[8] M. N. Do and M. Vetterli, "Framing pyramids," *IEEE Trans. Signal Process.*, vol. 51, pp. 2329–2342, September 2003.

[9] E. J. Candes and D. L. Donoho, "Recovering edges in ill-posed inverse problems: Optimality of curvelet frames," *Ann. Statist.*, vol. 30, no. 3, pp. 784–842, June 2002.

[10] D. L. Donoho, "Wedgelets: Nearly minimax estimation of edges," *Ann. Statist.*, vol. 27, no. 3, pp. 859–897, June 1998.

[11] S. Mallat and E. LePennec, "Sparse geometric image representation with bandelets," *IEEE Trans. Image Process.*, vol. 14, no. 4, pp. 423–438, April 2005.

[12] S. Mallat and Z. Zhang, "Matching pursuit in a time-frequency dictionary," *IEEE Trans. Signal Process.*, vol. 41, no. 12, pp. 3397–3415, December 1993.

[13] S. S. Chen, D. L. Donoho, and M. A. Saunders, "Atomic decomposition by basis pursuit," *SIAM Rev.*, vol. 43, no. 1, pp. 129–159, 2001.

[14] Priyam Chatterjee and Peyman Milanfar, "Clustering-Based Denoising With Locally Learned Dictionaries," *IEEE Trans. Image Process.*, vol. 18, no. 7, pp. 1438-1451, Jul. 2009.

[15] Y. C. Pati, R. Rezaiifar, and P. S. Krishnaprasad, "Orthogonal matching pursuit: Recursive function approximation with applications to wavelet decomposition," in *27th Annu. Asilomar Conf. Signals, Systems, and Computers*, 1993.

[16] M. De Marsico, M. Nappi , D. Riccio, and G. Tortora, "NABS: Novel Approaches for Biometric Systems," *IEEE Transactions on Systems, Man, and Cybernetics, Part C: Applications and Reviews*, vol. 41, no. 4, pp. 481-493, July 2011.

[17] Jianchao Yang, Zhaowen Wang, Zhe Lin, S. Cohen, and T. Huang, "Coupled Dictionary Training for Image Super-Resolution," *IEEE Trans. Image Process.*, vol. 21, no. 8, pp. 3467-3478, Aug. 2012.

[18] David L. Donoho, "For most large underdetermined systems of equations, the minimal ℓ1-norm near-solution approximates the sparsest near-solution," *Communications on Pure and Applied Mathematics*, vol. 59, no. 7, pp. 907-934, 2006.

[19] B. Efron, T. Hastie, I. Johnstone, and R. Tibshirani, "Least Angle Regression," *Annals of Statistics*, vol. 32, pp. 407-499, 2004.

[20] R. Tibshirani, "Regression shrinkage and selection via the lasso," *Journal of Royal Statistical Society, Series B*, vol. 58, no. 1, pp. 267-288, 1996.

[21] T. Arici, S. Dikbas, and Y. Altunbasak, "A Histogram Modification Framework and Its Application for Image Contrast Enhancement," *IEEE Trans. Image Process.*, vol. 18, no. 9, pp. 1921-1935, Sep. 2009.

[22] A.K. Jain, A. Ross, and S. Pankanti, "Biometrics: a tool for information security," *IEEE Trans. Information Forensics and Security*, vol. 1, no. 2, pp. 125-143, June 2006.

[23] H. Fronthaler, K. Kollreider, and J. Bigun, "Local Features for Enhancement and Minutiae Extraction in Fingerprints," *IEEE Trans. Image Process.*, vol. 17, no. 3, pp. 354-363, Mar. 2008.

[24] Antoni Buades, Bartomeu Coll, and Jean-Michel Morel, "A review of image denoising algorithms,with a new one," *SIAM Journal on Multiscale Modeling and Simulation: A SIAM Interdisciplinary Journal*, vol. 4, no. 2, pp. 490-530, 2005.

[25] N. Wiener, *Extrapolation, Interpolation, and Smoothing of Stationary Time Series*. New York: Wiley, 1949.

[26] M. Lindenbaum, M. Fischer, and A.M. Bruckstein, "On gabor contribution to image enhancement," *Pattern Recognition*, vol. 27, pp. 1–8, 1994.

[27] P. Perona and J. Malik, "Scale space and edge detection using anisotropic diffusion," *IEEE Trans. Patt. Anal.Mach. Intell.*, vol. 12, pp. 629-639, July 1990.

[28] L. Rudin and S. Osher, "Total variation based image restoration with free local constraints," in *IEEE Int. Conf. on Image Processing*, Texas, 1994, pp. 31–35.

[29] A. Buades, B. Coll, and J.-M. Morel, "A non-local algorithm for image denoising," in *IEEE Computer Society Conference on Computer Vision and Pattern*

Recognition , vol. 2, 2005, pp. 60-65.

[30] M. Mahmoudi and G. Sapiro, "Fast image and video denoising via nonlocal means of similar neighborhoods," *IEEE Signal Process. Lett.*, vol. 12, no. 12, pp. 839-842, Dec 2005.

[31] P. Coupe et al., "An optimized blockwise nonlocal means denoising filter for 3-d magnetic resonance images," *IEEE Trans. Med. Imag.*, vol. 27, no. 4, pp. 425-441, Apr 2008.

[32] T. Thaipanich, O. Byung Tae, W. Ping-Hao, X. Daru, and C. C. J. Kuo, "Improved image denoising with adaptive nonlocal means (anl-means) algorithm," *IEEE Trans. Consum. Electron.*, vol. 56, no. 4, pp. 2623-2630, Nov. 2010.

[33] Jin Wang, Yanwen Guo, Yiting Ying, Yanli Liu, and Qunsheng Peng, "Fast Non-Local Algorithm for Image Denoising," in *IEEE International Conference on Image Processing*, Atlanta, GA, 2006, pp. 1429-1432.

[34] S.G. Chang, Bin Yu, and M. Vetterli, "Adaptive wavelet thresholding for image denoising and compression," *IEEE Trans. Image Process.*, vol. 9, no. 9, pp. 1532-1546, Sep. 2000.

[35] M. Kivanc Mihcak, I. Kozintsev, K. Ramchandran, and P. Moulin, "Low-complexity image denoising based on statistical modeling of wavelet coefficients," *IEEE Signal Processing Letters*, vol. 6, no. 12, pp. 300-303, December 1999.

[36] Levent Sendur and I.W. Selesnick, "Bivariate shrinkage functions for wavelet-based denoising exploiting interscale dependency," *IEEE Trans. Signal Process.*, vol. 50, no. 11, pp. 2744-2756, Nov. 2002.

[37] J. Portilla, V. Strela, M.J. Wainwright, and E.P. Simoncelli, "Image denoising using scale mixtures of Gaussians in the wavelet domain," *IEEE Trans. Image Process.*, vol. 12, no. 11, pp. 1338-1351, Nov. 2003.

[38] M. Miller and Nick Kingsbury, "Image Denoising Using Derotated Complex Wavelet Coefficients," *IEEE Trans. Image Process.*, vol. 17, no. 9, pp. 1500-1511, Sep. 2008.

[39] J. L. Starck, E. J. Candes, and D. L. Donoho, "The curvelet transform for image denoising," *IEEE Trans. Image Process.*, vol. 11, no. 6, pp. 670–684, June 2002.

[40] M. N. Do and M. Vetterli, "The contourlet transform:An efficient directional multiresolution image representation," *IEEE Trans. Image Process.*, vol. 14, no. 12, pp. 2091-2106, Dec. 2005.

[41] E. Pennec and S. Mallat, "Sparse geometric image representations with bandelets," *IEEE Trans. Image Process.*, vol. 14, no. 4, pp. 423-438, Apr. 2005.

[42] Michal Aharon, Michael Elad, and Alfred Bruckstein, "K-SVD: An Algorithm for Designing Overcomplete Dictionaries for Sparse Representation," *IEEE Trans. Signal Process.*, vol. 54, no. 11, pp. 4311-4322, Nov. 2006.

[43] Julien Mairal, Guillermo Sapiro, and Michael Elad, "Learning Multiscale Sparse Representations for Image and Video Restoration," *Multiscale Modeling & Simulation*, vol. 7, no. 1, pp. 214-241 , April 2008.

[44] Xiaoqiang Lu, Yuan Yuan, and Pingkun Yan, "Sparse coding for image denoising using spike and slab prior," *Neurocomputing*, vol. 106, pp. 12-20, April 2013.

[45] Xuande Zhang, Xiangchu Feng, Weiwei Wanga, and Guojun Liu, "Image denoising via 2D dictionary learning and adaptive hard thresholding," *Pattern Recognition Letters*, vol. 34, pp. 2110–2117, 2013.

[46] Shuyuan Yang, Linfang Zhao, Min Wang, and Yueyuan Zhan, "Dictionary learning and similarity regularization based image noise reduction," *Journal of Vis. Comm. and Image Repr.*, vol. 24, no. 2, pp. 181-186, Feb. 2013.

[47] K. Dabov, A. Foi, V. Katkovnik, and K. Egiazarian, "Image Denoising by Sparse 3-D Transform-Domain Collaborative Filtering," *IEEE Trans. Image Process.*, vol. 16, no. 8, pp. 2080-2095, Aug. 2007.

[48] R. Keys, "Cubic convolution interpolation for digital image processing," *IEEE Trans. Acoustics, Speech and Signal Processing*, vol. 29, no. 6, pp. 1153-1160, Dec. 1981.

[49] X. Li and M. T. Orchard, "New edge-directed interpolation," *IEEE Trans. Image Process.*, vol. 10, no. 10, pp. 1521–1527, Oct. 2001.

[50] S. Mallat and G. Yu, "Super-resolution with sparse mixing estimators," *IEEE Trans. Image Process.*, vol. 19, no. 11, pp. 2889–2900, Nov. 2010.

[51] X. Zhang and X. Wu, "Image interpolation by adaptive 2-d autoregressive modeling and soft-decision estimation," *IEEE Trans. Image Process.*, vol. 17, no. 6, pp. 887–896, Jun. 2008.

[52] S. Baker and T. Kanade, "Limits on super-resolution and how to break them," *IEEE Trans. Pattern Anal. Mach. Intell.*, vol. 24, no. 9, pp. 1167–1183, Sep. 2002.

[53] M. Irani and S. Peleg, "Motion analysis for image enhancement: Resolution,occlusion and transparency," *J. Vis. Commun. Image Represent.*, vol. 4, no. 4, pp. 324–335, 1993.

[54] Z. C. Lin and H. Y. Shum, "Fundamental limits of reconstruction-based superresolution algorithms under local translation," *IEEE Trans. Pattern Anal. Mach. Intell.*, vol. 26, no. 1, pp. 83–97, Jan. 2004.

[55] Xiang Ma, Hiêp Quang Luong, Wilfried Philips, Huansheng Song, and Hua Cui, "Sparse representation and position prior based face hallucination upon classified over-complete dictionaries," *Signal Processing*, vol. 92, no. 9, pp. 2066-2074, September 2012.

[56] H. Chang, D.Y. Yeung, and Y. Xiong, "Super-resolution through neighbor embedding," in *IEEE International Conference on Computer Vision and Pattern Recognition*, Washington, D.C., 2004, pp. 275–282.

[57] W.T. Freeman, T.R. Jones, and E.C. Pasztor, "Example-based super-resolution," *Computer Graphics and Applications,IEEE* , vol. 22, no. 2, pp. 56-65, Mar/Apr 2002.

[58] W.T. Freeman, E.C. Pasztor, and O.T. Carmichael, "Learning low level vision," *Int. J. Comput. Vis.*, vol. 40, pp. 25–47, 2000.

[59] J. Wang, S. Zhu, and Y. Gong, "Resolution enhancement based on learning the sparse association of image patches," *Pattern Recognit.Lett.*, vol. 31, pp. 1–10, 2010.

[60] Weirong Liu and Shutao Li, "Multi-morphology image super-resolution via sparse representation," *Neurocomputing*, vol. 120, pp. 645-654, November 2013.

[61] Andrea Rueda, Norberto Malpica, and Eduardo Romero, "Single-image super-resolution of brain MR images using overcomplete dictionaries," *Medical image analysis*, vol. 17, no. 1, pp. 113–132, October 2012.

[62] Shuyuan Yang, Zhizhou Liu, Min Wang, and Fenghua Sun, "Multitask dictionary learning and sparse representation based single-image super-resolution reconstruction," *Neurocomputing*, vol. 74, no. 17, pp. 3193-3203, October 2011.

[63] Hai-cang Liu, Shu-tao Li, and Hai-tao Yin, "Infrared surveillance image super resolution via group sparse representation," *Optics Communications*, vol. 289, pp. 45-52, February 2013.

[64] Shuyuan Yang, Min Wang, Yaxin Sun, Fenghua Sun, and Licheng Jiao, "Compressive Sampling based Single-Image Super-resolution Reconstruction by dual-sparsity and Non-local Similarity Regularizer," *Pattern Recognition Letters*, vol. 33, no. 9, pp. 1049-1059, July 2012.

[65] Yi Tang, Yuan Yuan, Pingkun Yan, and Xuelong Li, "Greedy regression in sparse coding space for single-image super-resolution," *Journal of Vis. Comm. and Image Repr.*, vol. 24, no. 2, pp. 148-159, Feb. 2013.

[66] Shuyuan Yang, Yaxin Sun, Yiguang Chen, and Licheng Jia, "Structural similarity regularized and sparse coding based super-resolution for medical images," *Biomedical Signal Processing and Control*, vol. 7, no. 6, pp. 579-590, November 2012.

[67] R. Zeyde, M. Elad, and M. Protter, "On single image scale-up using sparse-representations," in *Proc. 7th Int. Conf. Curves Surfaces*, 2010, pp. 711–730.

[68] Zhiliang Zhu, Fangda Guo, Hai Yu, and Chen Chen, "Fast Single Image Super-Resolution via Self-Example Learning and Sparse Representation," *IEEE Trans. on Multimedia*, vol. 16, no. 8, pp. 2178-2190, Dec. 2014.

[69] Xiaoqiang Lu, Zihan Huang, and Yuan Yuan, "MR image super-resolution via manifold regularized sparse learning," *Neurocomputing*, vol. 162, pp. 96–104, 2015.

[70] Jian Lu and Yi Sun, "Context-aware single image super-resolution using sparse

representation and cross-scale similarity," *Signal Processing: Image Communication*, vol. 32 , pp. 40–53, 2015.

[71] Toshiyuki Kato, Hideitsu Hino, and Noboru Murataa, "Multi-frame image super resolution based on sparse coding," *Neural Networks*, vol. 66 , pp. 64–78, 2015.

[72] Yongqin Zhang, Jiaying Liu, Wenhan Yang, and Zongming Guo, "Image Super-Resolution Based on Structure-Modulated Sparse Representation," *IEEE Trans. Image Process.*, vol. 24, no. 9, pp. 2797-2810, Sep. 2015.

[73] L. Hong, Yifei Wan, and A. Jain, "Fingerprint image enhancement: algorithm and performance evaluation," *IEEE Trans. Pattern Anal. Mach. Intell.*, vol. 20, no. 8, pp. 777-789, Aug. 1998.

[74] Jianwei Yang, Lifeng Liu, Tianzi Jiang, and Yong Fan, "A modified Gabor filter design method for fingerprint image enhancement," *Pattern Recognition Letters*, vol. 24, no. 12, pp. 1805-1817, Aug. 2003.

[75] Wei Wang, Jianwei Li, Feifei Huang, and Hailiang Feng, "Hailiang Feng, Design and implementation of Log-Gabor filter in fingerprint image enhancement," *Pattern Recognition Letters*, vol. 29, no. 3, pp. 301-308, February 2008.

[76] Ching-Tang Hsieh, Eugene Lai, and You-Chuang Wang, "An effective algorithm for fingerprint image enhancement based on wavelet transform," *Pattern Recognition*, vol. 36, no. 2, pp. 303-312, February 2003.

[77] B.G. Sherlock, D.M. Monro, and K. Millard, "Fingerprint enhancement by directional Fourier filtering," in *Vision, Image and Signal Processing, IEE Proceedings*, vol. 141, 1994, pp. 87-94.

[78] Jucheng Yang, Naixue Xiong, and A.V. Vasilakos, "Two-Stage Enhancement Scheme for Low-Quality Fingerprint Images by Learning From the Images," *IEEE Trans. Human-Machine Systems*, vol. 43, no. 2, pp. 235-248, March 2013.

[79] Lawrence O'Gorman and Jeffrey V. Nickerson, "An approach to fingerprint filter design," *Pattern Recognition*, vol. 22, no. 1, pp. 29-38, 1989.

[80] Shlomo Greenberg, Mayer Aladjem, and Daniel Kogan, "Fingerprint Image Enhancement using Filtering Techniques," *Real-Time Imaging*, vol. 8, no. 3, pp. 227-236, June 2002.

[81] A. Almansa and T. Lindeberg, "Fingerprint enhancement by shape adaptation of scale-space operators with automatic scale selection," *IEEE Trans. Image Process.*, vol. 9, no. 12, pp. 2027-2042, Dec. 2000.

[82] Jiangang Cheng and Jie Tian, "Fingerprint enhancement with dyadic scale-space," *Pattern Recognition Letters*, vol. 25, no. 11, pp. 1273-1284, August 2004.

[83] M. Tico, V. Onnia, and P. Kuosmanen, "Fingerprint Image Enhancement Based on Second Directional Derivative of the Digital Image," *EURASIP J. Appl. Signal Process., vol. 2002, no. 10, p. ,.*, vol. 2002, no. 10, pp. 1135–1144, October 2002.

[84] Zhi Yuan, Jiong Wu, S. Kamata, A Ahrary, and Peimin Yan, "Fingerprint image enhancement by super resolution with early stopping," , vol.4, no., pp.," in *IEEE International Conference on Intelligent Computing and Intelligent Systems*, vol. 4, 2009, pp. 527-531.

[85] C.V. Jiji and S. Chaudhuri, "PCA-based generalized interpolation for image super-resolution," in *Proceedings of Indian Conference on Vision , Graphics & Image Processing*, 2004, pp. 139-144.

[86] R. C. Gonzalez and R. E. Woods, *Digital Image Processing*, 3rd ed. NJ, US: Prentice Hall, 2008.

[87] Yeong-Taeg Kim, "Contrast Enhancement Using Brightness Preserving Bi-Histogram Equalization," *IEEE Trans. Consumer Electron.*, vol. 43, no. 1, pp. 1-8, 1997.

[88] Yu Wang, Qian Chen, and Baomin Zhang, "Image enhancement based on equal area dualistic sub-image histogram equalization method," *IEEE Trans. Consumer Electron.*, vol. 45, no. 1, pp. 68-75, 1999.

[89] Soong-Der Chen and Abd. Rahman Ramli, "Minimum Mean Brightness Error Bi-Histogram Equalization in Contrast Enhancement," *IEEE Trans. Consumer Electron.*, vol. 49, no. 4, pp. 1310-1319, 2003.

[90] Soong-Der Chen and Abd. Rahman Ramli, "Contrast Enhancement using Recursive Mean-Separate Histogram Equalization for Scalable Brightness

Preservation," *IEEE Trans. Consumer Electron.*, vol. 49, no. 4, pp. 1301-1309, 2003.

[91] K.S. Sim, C.P. Tso, and Y.Y. Tan, "Recursive sub-image histogram equalization applied to gray scale images," *Pattern Recognition Letters* , vol. 28 , pp. 1209–1221, 2007.

[92] Mary Kim and Min Gyo Chung, "Recursively Separated and Weighted Histogram Equalization for Brightness Preservation and Contrast Enhancement," *IEEE Trans. Consumer Electron.*, vol. 54, no. 3, pp. 1389-1397, 2008.

[93] Qing Wang and Rabab K. Ward, "Fast Image/Video Contrast Enhancement Based on Weighted Thresholded Histogram Equalization," *IEEE Trans. Consumer Electron.*, vol. 53, no. 2, pp. 757-764, May 2007.

[94] Taekyung Kim and Joonki Paik, "Adaptive Contrast Enhancement Using Gain-Controllable Clipped Histogram Equalization," *IEEE Trans. Consumer Electron.*, vol. 54, no. 4, pp. 1803-1810, 2008.

[95] Chen Hee Ooi, Nicholas Sia Pik Kong, and Haidi Ibrahim, "Bi-Histogram Equalization with a Plateau Limit for Digital Image Enhancement," *IEEE Trans. Consumer Electron.*, vol. 55, no. 4, pp. 2072-2080, 2009.

[96] M. Abdullah-Al-Wadud, Md. Hasanul Kabir, M. Ali Akber Dewan, and Oksam Chae, "A Dynamic Histogram Equalization for Image Contrast Enhancement," *IEEE Trans. on Consumer Electronics*, vol. 53, no. 2, pp. 593-600, 2007.

[97] Haidi Ibrahim and Nicholas Sia Pik Kong, "Brightness Preserving Dynamic Histogram Equalization for Image Contrast Enhancement," *IEEE Trans. Consumer Electron.*, vol. 53, no. 4, pp. 1752-1758, 2007.

[98] Debdoot Sheet, Hrushikesh Garud, Amit Suveer, Manjunatha Mahadevappa, and Jyotirmoy Chatterjee, "Brightness Preserving Dynamic Fuzzy Histogram Equalization," *IEEE Trans. Consumer Electron.*, vol. 56, no. 4, pp. 2475-2480, 2010.

[99] David Menotti, Laurent Najman, Jacques Facon, and Arnaldo de A. Araújo, "Multi-Histogram Equalization Methods for Contrast Enhancement and Brightness Preserving," *IEEE Trans. Consumer Electron.*, vol. 53, no. 3, pp. 1186-1194, Aug. 2007.

[100] Gyu-Hee Park, Hwa-Hyun Cho, and Myung-Ryul Choi, "A Contrast Enhancement Method using Dynamic Range Separate Histogram Equalization," *IEEE Trans. Consumer Electron.*, vol. 54, no. 4, pp. 1981-1987, Nov. 2008.

[101] Chen Hee Ooi and Nor Ashidi Mat Isa, "Quadrants Dynamic Histogram Equalization for Contrast Enhancement," *IEEE Trans. Consumer Electron.*, vol. 56, no. 4, pp. 2552-2559, 2010.

[102] Chen Hee Ooi and Nor Ashidi Mat Isa, "Adaptive Contrast Enhancement Methods with Brightness Preserving," *IEEE Trans. Consumer Electron.*, vol. 56, no. 4, pp. 2543-2551, 2010.

[103] Nyamlkhagva Sengee and Heung Kook Choi, "Brightness Preserving Weight Clustering Histogram Equalization," *IEEE Trans. Consumer Electron.*, vol. 54, no. 3, pp. 1329-1337, Aug. 2008.

[104] Yen-Ching Chang and Chun-Ming Chang, "A Simple Histogram Modification Scheme for Contrast Enhancement," *IEEE Trans. Consumer Electron.*, vol. 56, no. 2, pp. 737-742, 2010.

[105] A.K. Jain, S. Prabhakar, L. Hong, and S. Pankanti, "Filter bank-based fingerprint matching," *IEEE Trans. Image Process.*, vol. 9, no. 5, pp. 846-859, May 2000.

[106] A.K. Jain, S. Prabhakar, and S. Pankanti, "A Filterbank-based Representation for Classification and Matching of Fingerprints," in *International Joint Conference on Neural Networks*, vol. 5, 1999, pp. 3284-3285.

[107] XiaoGuang Feng and P. Milanfar, "Multiscale principal components analysis for image local orientation estimation," in *Asilomar Conf. on Signals, Systems and Computers*, 2002, pp. 478-482.

[108] Zhou Wang, A.C. Bovik, H.R. Sheikh, and E.P. Simoncelli, "Image quality assessment: from error visibility to structural similarity," *IEEE Trans. Image Process.*, vol. 13, no. 4, pp. 600-612, Apr. 2004.

[109] Kuldeep Singh, Rajiv Kapoor, and Raunaq Nayar, "Fingerprint denoising using ridge orientation based clustered dictionaries," *Neurocomputing*, vol. 167, pp. 418-423, 2015.

[110] Kuldeep Singh, Anubhav Gupta, and Rajiv Kapoor, "Fingerprint image super-resolution via ridge orientation-based clustered coupled sparse dictionaries," *Journal of Electronic Imaging*, vol. 24, no. 4, pp. 043015-1-10, 2015.

[111] Kuldeep Singh and Rajiv Kapoor, "Image enhancement via Median-Mean Based Sub-Image-Clipped Histogram Equalization," *Optik*, vol. 125, pp. 4646–4651, 2014.

[112] Kuldeep Singh and Rajiv Kapoor, "Image enhancement using Exposure based Sub Image Histogram," *Pattern recognition letters*, vol. 36, pp. 10-14, 2014.

[113] Kuldeep Singh, Rajiv Kapoor, and Sanjeev Kr Sinha, "Enhancement of low exposure images via recursive histogram equalization algorithms," *Optik*, vol. 126, pp. 2619–2625, 2015.

[114] Soong-Der Chen, "A new image quality measure for assessment of histogram equalization-based contrast enhancement techniques," *Digital Signal Processing* , vol. 22, pp. 640–647, 2012.

AUTHOR BIOGRAPHY

Kuldeep Singh
Scientist , Central Research Lab, Bharat Electronics Ltd.
Ghaziabad , India
Email: kuldeep.er@gmail.com

Kuldeep Singh received his B.E. degree in Electronics & Comm. from Govt. Engg. College, Ajmer India in 2004 and M. Tech. degree in Signal Processing from Delhi University in 2006.He is currently pursuing PhD from Delhi Technological University, India. He works as scientist at Central Research Laboratory, Bharat Electronics Limited (Ministry of Defense, Government of India), India. He has published over 10 research papers in refereed journals and conference proceedings. His research interest includes image enhancement, sparse representation based image processing and pattern recognition. He is also reviewer of various Elsevier, Taylor & Francis, and IET journals.